nature immunology

Resource

https://doi.org/10.1038/s41590-024-02073-8

Signature cytokine-associated transcriptome analysis of effector γδ T cells identifies subset-specific regulators of peripheral activation

Received: 27 February 2024

Accepted: 20 December 2024

Published online: 29 January 2025

Check for updates

Daniel Inácio[1,2], Tiago Amado[1,9], Ana Pamplona[1,9], Daniel Sobral[3], Carolina Cunha[1], Rita F. Santos[4,5,6], Liliana Oliveira[4,5], Nelly Rouquié[7], Alexandre M. Carmo[4,5], Renaud Lesourne[7], Anita Q. Gomes[1,8,10] ✉ & Bruno Silva-Santos[1,2,10] ✉

γδ T cells producing either interleukin-17A (γδ^{17} cells) or interferon-γ (γδ^{IFN} cells) are generated in the mouse thymus, but the molecular regulators of their peripheral functions are not fully characterized. Here we established an *Il17a*-GFP:*Ifng*-YFP double-reporter mouse strain to analyze at unprecedented depth the transcriptomes of pure γδ^{17} cell versus γδ^{IFN} cell populations from peripheral lymph nodes. Within a very high fraction of differentially expressed genes, we identify a panel of 20 new signature genes in steady-state γδ^{17} cells versus γδ^{IFN} cells, which we further validate in models of experimental autoimmune encephalomyelitis and cerebral malaria, respectively. Among the signature genes, we show that the co-receptor CD6 and the signaling protein Themis promote the activation and proliferation of peripheral γδ^{IFN} cells in response to T cell antigen receptor stimulation in vitro and to *Plasmodium* infection in vivo. This resource can help to understand the distinct activities of effector γδ T cell subsets in pathophysiology.

The contribution of γδ T cell subsets to immune responses has been associated with either beneficial or pathogenic functions in disease settings[1,2]. Importantly, two effector γδ T cell subsets have distinct roles in the pathophysiology of severe malaria. First, using the well-established model of experimental cerebral malaria (ECM) based on *Plasmodium berghei* ANKA infection of C57BL/6 mice, γδ T cells were shown to orchestrate interferon-γ (IFNγ) responses across the liver–spleen axis that drives immunopathology in the central nervous system[3]. In particular, IFNγ$^+$ γδ T cells were required for ECM development under high parasite burdens and maximal IFNγ production by CD4$^+$ and CD8$^+$ T cells (required for ECM development in the central nervous system) and were able to transfer disease to ECM-resistant T cell antigen receptor-δ (TCRδ)-deficient mice. In stark contrast to this pathogenic function of IFNγ$^+$ γδ T cells, a subsequent study demonstrated that interleukin-17-positive (IL-17$^+$) γδ T cells have an important protective function following activation by low parasite burden in

[1]Gulbenkian Institute for Molecular Medicine, Lisbon, Portugal. [2]Faculdade de Medicina, Universidade de Lisboa, Lisbon, Portugal. [3]Instituto Nacional de Saúde Dr. Ricardo Jorge, Lisbon, Portugal. [4]Instituto de Investigação e Inovação em Saúde (i3S), Universidade do Porto, Porto, Portugal. [5]Instituto de Biologia Molecular e Celular (IBMC), Porto, Portugal. [6]ESS, Politécnico do Porto, Porto, Portugal. [7]Toulouse Institute for Infectious and Inflammatory Diseases (Infinity), INSERM UMR1291, CNRS UMR5051, University Toulouse III, Toulouse, France. [8]H&TRC Health and Technology Research Center, Escola Superior de Tecnologia da Saúde, Instituto Politécnico de Lisboa, Lisbon, Portugal. [9]These authors contributed equally: Tiago Amado, Ana Pamplona. [10]These authors jointly supervised this work: Anita Q. Gomes, Bruno Silva-Santos. ✉e-mail: anita.gomes@gimm.pt; bssantos@medicina.ulisboa.pt

the liver, producing IL-17 that is essential to induce 'emergency erythropoiesis' in the spleen, thus avoiding the hijacking of the erythroid system by *Plasmodium* and preventing the development of ECM[4]. These findings underline the importance of characterizing the molecular mechanisms that selectively control the differentiation and activation of each effector γδ T cell subset and their impact on pathophysiology.

Previous work from our laboratory and others has shown that these two effector γδ T cell subsets segregate early during thymic development based on distinct transcriptional, signaling and metabolic requirements[5,6]. In contrast to the delineation of important events and molecular mediators during thymic development, the factors that control the selective activation of IL-17$^+$ versus IFNγ$^+$ γδ T cells in the periphery are not well characterized. This notwithstanding, the reported effect of co-receptors CD27, PD-1 and TIM-3 shows the potential of molecules that are differentially expressed on effector γδ T cell subsets to control their functional response following challenge[7].

Previous studies used cell surface markers to isolate discrete subsets of γδ T cells but lacked a direct association with the production of signature cytokines[8,9]. Here we identify new molecular regulators of the effector γδ T cell subsets in the periphery in an unbiased manner and at the genome-wide level. To achieve unprecedented depth for analysis of the specific transcriptomes of IL-17$^+$ versus IFNγ$^+$ γδ T cells (here designated γδ^{17} and γδ^{IFN} cells, respectively), we established *Il17a*-GFP:*Ifng*-YFP double-reporter mice by crossing the single reporter strains *Il17a*-GFP and *Ifng*-YFP (Great) and purified the corresponding populations from pooled peripheral lymphoid organs for RNA sequencing (RNA-seq). This valuable resource of subset-specific gene expression profiles and their functional validation in distinct pathophysiological settings was used to identify new functions for the co-receptor CD6 and the signaling protein Themis in selectively regulating the activation of γδ^{IFN} cells following TCR stimulation in vitro and malaria infection in vivo.

Results

Divergence between pure γδ^{17} and γδ^{IFN} cell transcriptomes

Although cell surface markers and TCR variable γ-chain (Vγ) usage can enrich for IL-17- or IFNγ-producing γδ T cells, they fail to define 'pure' effector γδ T cells[8–10]. To overcome this limitation, we established a double-reporter mouse strain for the two signature cytokines, that is, *Il17a*-GFP:*Ifng*-YFP mice, by crossing previously available single-reporter strains (Fig. 1a). Flow cytometry sorting of peripheral lymph node (pLN) γδ T cells expressing green fluorescent protein (GFP) or yellow fluorescent protein (YFP) following a short-term (3-h) stimulation with phorbol 12-myristate 13-acetate (PMA) and ionomycin allowed us to confirm that essentially all GFP$^+$ versus YFP$^+$ γδ T cells express intracellular IL-17A or IFNγ, respectively (Fig. 1b–d and Extended Data Fig. 1a), thus validating them as 'pure' γδ^{17} and γδ^{IFN} subsets. These cells showed the expected TCR Vγ chain usage; that is, lymphoid γδ^{17} cells were Vγ4$^+$ (~85%) or Vγ1$^-$Vγ4$^-$ (~15%), likely Vγ6$^+$ cells, whereas γδ^{IFN} cells were composed of Vγ4$^+$ (~50%), Vγ1$^+$ (~30%) and Vγ1$^-$Vγ4$^-$ (~15%) cells (Extended Data Fig. 1b). Moreover, γδ^{17} cells were CD44^{high}CD45RB$^-$, whereas γδ^{IFN} cells were mostly CD44^{int}CD45RB$^+$, as previously described for mature IFNγ-producing γδ T cells[10] (Extended Data Fig. 1c). By contrast, CD44 and CD45RB staining alone failed to identify pure GFP$^+$ or YFP$^+$ γδ T cell subsets because only ~60% of CD44^{high} γδ T cells were *Il17a*-GFP$^+$, and, even more notably, less than 30% of CD45RB^{high} γδ T cells were *Ifng*-YFP$^+$ (Extended Data Fig. 1d). Similarly, although γδ^{17} (*Il17a*-GFP$^+$) and γδ^{IFN} (*Ifng*-YFP$^+$) cells were mostly CD27$^-$ and CD27$^+$, respectively, the sole use of CD27 staining failed to delineate pure γδ^{17} and γδ^{IFN} cells (Extended Data Fig. 1e,f). These data demonstrate the methodological advance of our *Il17a*:*Ifng* double-reporter strategy.

To characterize the transcriptomes of γδ^{17} and γδ^{IFN} cell subsets, we isolated total RNA from peripheral GFP$^+$ and YFP$^+$ γδ T cells and from GFP$^-$YFP$^-$ 'double negative' (γδ^{DN}) cells sorted by fluorescence-activated cell sorting (FACS) and performed next-generation sequencing (Fig. 1b). Principal component analysis (PCA) of the RNA-seq data showed that all three biological replicates of each subset clustered tightly together but very far apart from the other subsets, suggesting a strong divergence of their global transcriptomes (Fig. 1e), especially between the γδ^{17} and γδ^{IFN} subsets, whereas the γδ^{DN} population was closer to the γδ^{IFN} subset (Fig. 1f). To build on these data, we tested precursor–product relationships between γδ^{DN} cells and the two effector subsets in vitro. We sorted γδ^{DN} cells and cultured them overnight under γδ^{17} (that is, IL-1β plus IL-23) or γδ^{IFN} (IL-12 plus IL-18) differentiation conditions. Although treatment with IL-12 plus IL-18, independent of TCR stimulation, led to 70–80% γδ^{IFN} cells, treatment with IL-1β plus IL-23 induced very low frequencies of γδ^{17} cells, actually lower frequencies than γδ^{IFN} cells (Extended Data Fig. 1g), thus suggesting that γδ^{DN} cells are 'poised' to generate γδ^{IFN} rather than γδ^{17} cells.

We detected the expression of a total of 12,822 genes in γδ T cells (Fig. 1g), with a greater number of genes (555) being expressed specifically in γδ^{17} cells compared with γδ^{IFN} (220) and γδ^{DN} cells (248). Among the 7,250 genes found to be differentially expressed overall, 13% (936 genes) were differentially expressed across all subsets, 25% (1,810 genes) were differentially expressed between γδ^{DN} and γδ^{IFN} cells, 70% (5,102 genes) were differentially expressed between γδ^{DN} and γδ^{17} cells, and 87% (6,308) were differentially expressed between γδ^{17} and γδ^{IFN} cells (Fig. 1h). This meant that, at this depth of RNA-seq, a striking 49% of all genes expressed in γδ T cells were differentially expressed between their two main effector subsets, with γδ^{17} cells clearly diverging not only from γδ^{IFN} cells but also from γδ^{DN} cells. Of note, all samples had a similar count of around 40 million reads, indicating that the observed differences are not influenced by variations in read numbers. All the differentially expressed genes between γδ^{17} and γδ^{IFN}, γδ^{17} and γδ^{DN} and γδ^{IFN} and γδ^{DN} cells are listed on Supplementary Tables 1–3, respectively.

Gene families and pathways enriched in γδ^{17} versus γδ^{IFN} cells

The volcano plots derived from the RNA-seq data highlighted well-established signature genes of the effector γδ T cell subsets, like *Il17a*, *Rorc* and *Il23r* overexpressed in γδ^{17} cells and *Ifng*, *Ccl5* and *Ccl9* upregulated in γδ^{IFN} cells (Fig. 1i–k). We next performed a detailed and targeted analysis of the gene families to which these signature genes belong (cytokines, cytokine and chemokine receptors and transcription factors). This analysis showed that *Il17a*, *Il17f*, *Il23r*, *Ccr6* and *Rorc* are the most enriched transcripts in γδ^{17} cells (top regions of the heat maps in Fig. 2a–c), whereas *Ifng*, *Ccl5*, *Ccl9*, *Ccr7* and *Eomes* (bottom regions of the heat maps in Fig. 2a–c) are the most γδ^{IFN} biased.

For broader biological insight, we performed an unbiased analysis of all genes differentially expressed between γδ^{17} and γδ^{IFN} cells, which segregated into four clusters, two enriched in γδ^{IFN}-biased genes related to translation and ribosome metabolism and two enriched in γδ17-biased genes related to signal transduction (Fig. 2d,e). More specifically, transcription and translation activities, including genes encoding proteins involved in translation and ribosomal biogenesis and structure and activity, stood out in γδ^{IFN} cells, whereas multiple receptors and signaling pathways linked to cytoskeleton remodeling and cell–cell communication were enriched in γδ^{17} cells, suggesting that they are particularly equipped to sense and integrate external cues (Fig. 2e).

To further increase the granularity of our RNA-seq data, we resorted to the KEGG database and tested for pathways enriched in γδ^{17} versus γδ^{IFN} cells. A total of 106 KEGG pathways were significantly represented in γδ^{17} cells. Not focusing on those generically related with diseases, we noted a total of 62 biological pathways (Supplementary Table 4), grouped in the KEGG classes summarized in Supplementary Table 5. The class with a higher number of pathways represented was 'environmental information processing' (signal transduction pathways), followed by classes under 'organismal systems', which, besides the immune system, interestingly included the endocrine and nervous systems. There were also several pathways pertaining to

https://doi.org/10.1038/s41590-024-02073-8

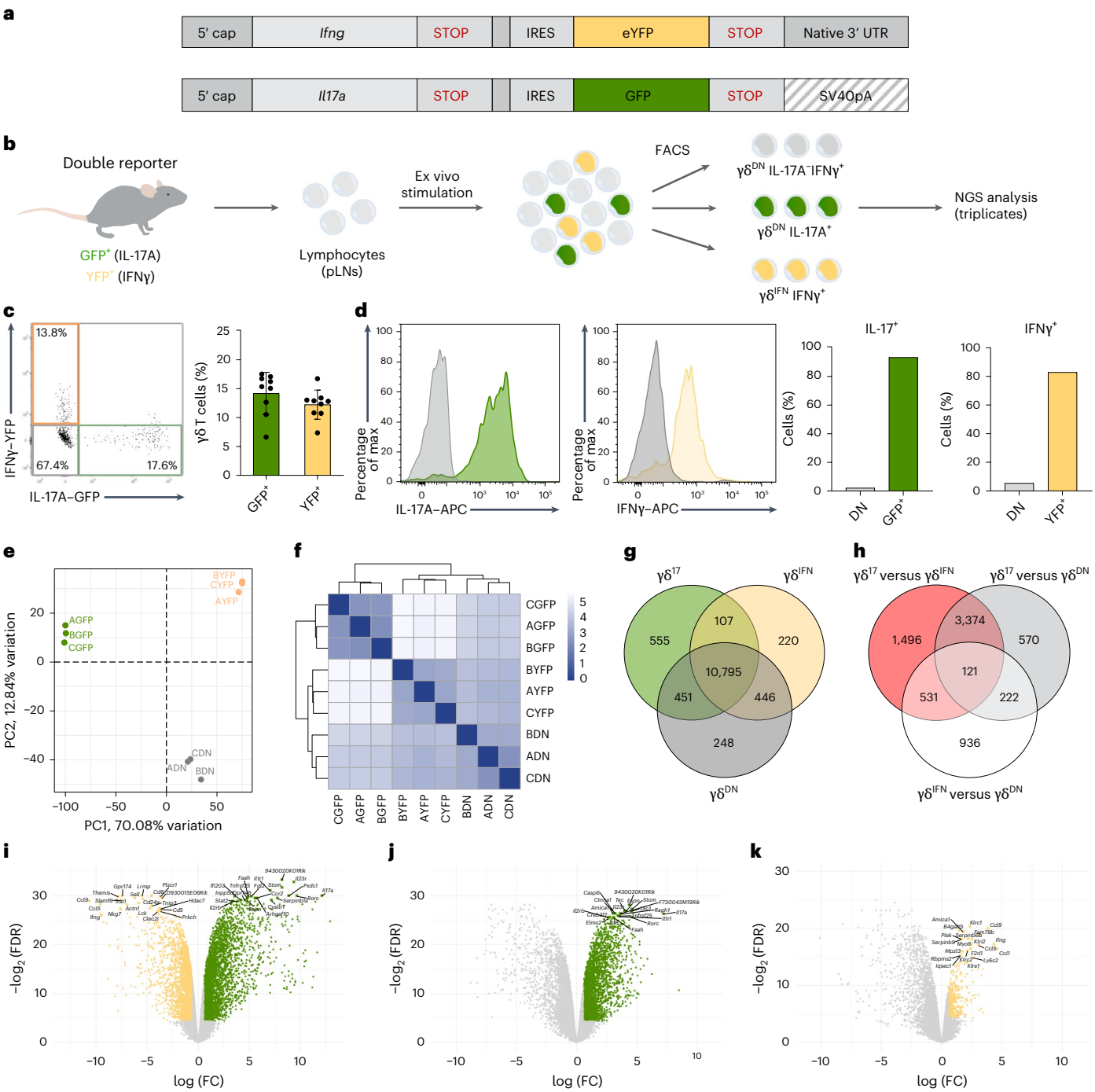

Fig. 1 | Characterization of the divergent transcriptomes of γδ^{17} versus γδ^{IFN} cells. a, Schematic of the genomic alterations introduced in the double-reporter *Il17a*-GFP:*Ifng*-YFP mouse strain used for isolation of γδ^{17} and γδ^{IFN} cells. In each cytokine locus, a sequence for an independently translated fluorescent reporter protein was inserted downstream of the cytokine's endogenous translational stop codon; UTR, untranslated region. **b**, Graphical overview of the protocol used to isolate the populations of interest. In short, cells were isolated from the pLNs of *Il17a*-GFP:*Ifng*-YFP reporter mice stimulated with PMA plus ionomycin and sorted by FACS accordingly to their fluorescence profiles; NGS, next-generation sequencing. **c**, Average proportion of GFP$^+$ and YFP$^+$ γδ T cells obtained by FACS (right; $n = 9$, three independent experiments) with a representative plot (left). **d**, Intracellular staining of IL-17 and IFNγ on sorted GFP$^+$ or YFP$^+$ γδ T cells. **e**, PCA plot of all nine samples used for RNA-seq data analysis based on normalized expression values. Each population of cells isolated (GFP$^+$YFP$^-$ (labeled GFP), GFP$^-$YFP$^+$ (labeled YFP) and GFP$^-$YFP$^-$ (labeled DN)) is represented by three independent samples labeled A, B and C, each composed of a pool of cells from several mice. **f**, Distance matrix showing the Euclidean distance of the different samples comparing normalized expression values (CPMs). Samples are clustered using hierarchical clustering. **g**, Venn diagram of expressed genes (defined as having a normalized CPM value of >1 in at least two of three samples of the group) in the different subsets. **h**, Venn diagram of differentially expressed genes (false discovery rate (FDR) of <0.05 and fold change of >1.5) of the different comparison pairs. **i**–**k**, Volcano plots displaying the $\log_2$ (fold change) and $\log_2$ (FDR) resulting from a differential expression analysis comparing GFP$^+$ versus YFP$^+$ (**i**), GFP$^+$ versus DN (**j**) and YFP$^+$ versus DN (**k**). Some of the most significantly differentially expressed genes are annotated, focusing on genes selectively enriched in GFP$^+$ (γδ^{17}) or YFP$^+$ (γδ^{IFN}) cells. Data are shown as mean ± s.d. (**c**); FC, fold change.

https://doi.org/10.1038/s41590-024-02073-8

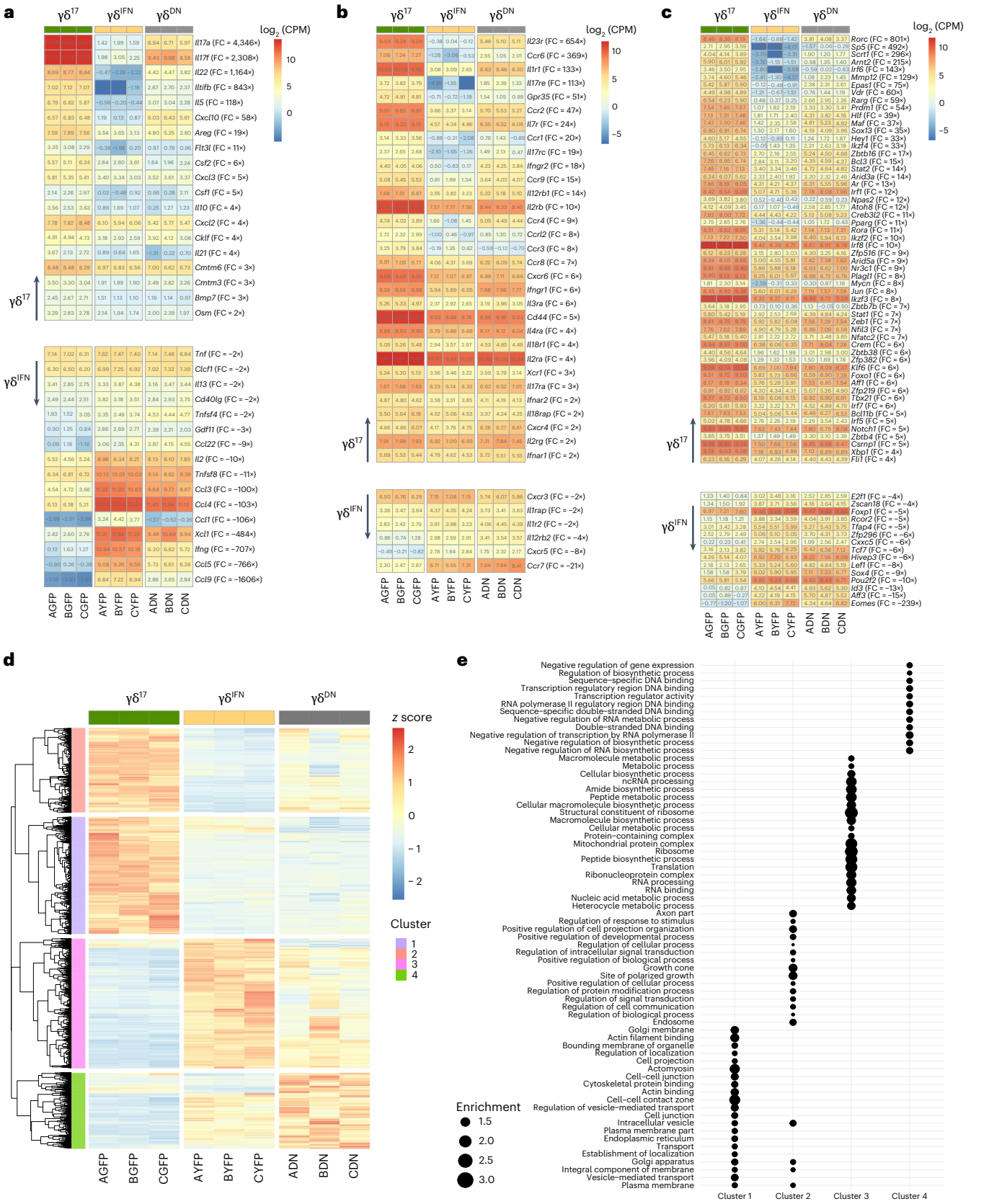

Fig. 2 | Gene families and pathways enriched in peripheral γδ^{17} versus γδ^{IFN} cells. a–**c**, Heat maps displaying the $\log_2$ (CPM) normalized expression values of differentially expressed genes more expressed in γδ^{17} (top) or in γδ^{IFN} (bottom) cells for cytokines (**a**), cytokine and chemokine receptors (**b**) and transcription factors (**c**). **d**, Heat map displaying the row-scaled *z* scores of normalized expression values of all differentially expressed genes. Genes were clustered using hierarchical clustering, and a cutting point was selected to obtain four groups. **e**, Gene Ontology (GO) terms significantly enriched in a GO enrichment analysis using GoRilla comparing the GO annotations of genes present in each individual cluster to annotations of the genes of all clusters.

the metabolism of carbohydrates, lipids and glycan biosynthesis and metabolism, none of which were detected in γδ^{IFN} cells. Conversely, these were enriched for 39 pathways, 12 disease-related pathways and 27 biological pathways listed in Supplementary Table 6 grouped into KEGG classes shown in Supplementary Table 7. γδ^{IFN} cell-biased pathways included processes related to DNA and RNA metabolism, namely replication and repair, transcription and translation and nucleotide metabolism. Overall, these pathway analyses revealed substantial differences between γδ^{17} and γδ^{IFN} cells beyond their different cytokine-producing patterns, which we sought to examine further at the gene level.

Identification of signature genes in γδ^{17} versus γδ^{IFN} cells

We next aimed to identify new signature genes in γδ^{17} versus γδ^{IFN} cells, that is, highly differentially expressed genes thus far unknown to distinguish the two effector γδ T cell subsets. We focused on the top 50 differentially expressed genes between γδ^{17} and γδ^{IFN} cells (Fig. 3a,b). Besides the known hallmark genes (including *Il17a* and *Ifng*) that were already identified in the volcano plot of Fig. 1i, there were many unappreciated genes, for which we required additional insight. We took advantage of a parallel RNA-seq analysis performed in our laboratory on corresponding effector CD4$^+$ T cell subsets isolated from similar reporter mice at the peak of experimental autoimmune encephalomyelitis (EAE; SRA-SUB14032445), given that type 1 helper T (T_H1) cells and IL-17-producing helper T (T_H17) cells are not readily found at steady state but require an inflammatory challenge for their differentiation and expansion[11]. At the global level, it was interesting to observe that γδ^{17} and γδ^{IFN} cells were markedly further apart from each other (at the level of the second component of the PCA analysis) than T_H17 and T_H1 cells (Extended Data Fig. 2a), which was associated with much higher numbers of differentially expressed genes between γδ T cell subsets than the corresponding CD4$^+$ T cell subsets (Extended Data Fig. 2b,c). More specifically, we used these parallel RNA-seq analyses to analyze the expression of the top 50 differentially expressed genes between γδ^{17} and γδ^{IFN} cells in their T_H17 and T_H1 counterparts. Strikingly, with the exception of the known hallmark genes, the vast majority of the top 50 γδ^{17}/γδ^{IFN} candidates were not differentially expressed between T_H17 and T_H1 cells (Extended Data Fig. 2d,e), suggesting a unique relevance in effector γδ T cell subsets.

As final criteria for γδ^{17}/γδ^{IFN} signature genes among the top 50 candidates, we focused on those with known biological functions that exhibited an average normalized read count (counts per million (CPM)) higher than 30 (to be above very low expression levels) in the RNA-seq analysis of the γδ T cell subsets. This resulted in the selection of 13 genes associated with γδ^{17} cells and 13 genes associated with γδ^{IFN} cells, besides 5 hallmark genes encoding cytokines/cytokine receptors that we kept in our γδ^{17}/γδ^{IFN} signature panel for reference: *Il17a*, *Il22* and *Il23r* for γδ^{17} cells and *Ifng* and *Il2* for γδ^{IFN} cells (Fig. 3c,d). Among the 26 signature genes, we found some encoding distinct chemokines with a very strong presence (*Ccl3*, *Ccl4*, *Ccl5*, *Ccl9* and *Xcl1*) in γδ^{IFN} cells (Fig. 3d) and two other interesting biases. γδ^{17} cell signature genes included genes encoding enzymes (*Adam12* and *Ptgs2*), membrane channels (*Aqp3*) and neuroreceptors (*Ret*; Fig. 3c), which were consistent with the concept of sensing and integrating external cues (Fig. 2e and Supplementary Table 5), whereas γδ^{IFN} signature genes contained multiple genes associated with TCR signaling (*Themis*, *Slamf6*, *Cd5* and *Cd6*) or its regulation (*Lag3* and *Cd160*; Fig. 3d), aligned with the pathways involved in cell proliferation (Supplementary Table 7). Collectively, these data provide a new conceptual framework to understand and study the functional differences between γδ^{17} and γδ^{IFN} cells, including 26 potential signature genes whose pattern of expression we sought to characterize and validate further.

Signature gene expression in steady state and disease

TCR Vγ usage has been used for decades as a means to distinguish γδ T cell subsets with different ontogeny, tissue tropism and functional properties[1,12]. Regarding γδ^{17} and γδ^{IFN} cells, it has become clear that each harbor two main Vγ-based subpopulations, as confirmed in this study on the sorted pLN γδ T cell subsets (Extended Data Fig. 1b). To assess how the expression levels of the new signature genes might vary with Vγ usage within γδ^{17} or γδ^{IFN} cells, we sorted four populations from pooled spleens and pLNs of *Il17a*-GFP:*Ifng*-YFP mice: Vγ4$^+$ and Vγ1$^-$Vγ4$^-$ (largely Vγ6$^+$) GFP$^+$ (that is, γδ^{17}) cells and Vγ1$^+$ and Vγ4$^+$YFP$^+$ (that is, γδ^{IFN}) cells. We then performed quantitative PCR with reverse transcription (RT–qPCR) using a set of optimized specific primers provided in Methods. The results confirmed (as independent validation of the RNA-seq) the clear-cut segregation of all these genes as either γδ^{17} or γδ^{IFN} signature genes, with generally minor differences between the Vγ-based subpopulations of γδ^{17} and γδ^{IFN} cells (Extended Data Fig. 3a–c). Notwithstanding, we noted that γδ^{17} cells tended to be more heterogenous than γδ^{IFN} cells, as half of the 16 γδ^{17} signatures were differentially expressed between the Vγ4$^+$ and Vγ1$^-$Vγ4$^-$ (Vγ6$^+$) subpopulations (Extended Data Fig. 3b,c). Given the different thymic ontogeny of Vγ4$^+$ and Vγ6$^+$ cells, we next questioned the impact of the thymus on the expression levels of signature genes. This is particularly relevant because γδ^{17} and γδ^{IFN} cells can be functionally programmed in the thymus before homing to multiple peripheral organs[1,5]. To address this issue, we sorted both populations from the thymus, spleen and pLNs of the same *Il17a*-GFP:*Ifng*-YFP mice and performed a new set of RT–qPCR analyses (Fig. 4a,b), which provided multiple insights. First, all five γδ^{17}/γδ^{IFN} hallmark genes were validated as strong differentials across all organs, which constituted an important quality control. Second, 6 of the 13 γδ^{17}-biased genes (*Cxcl10*, *Ltbr4*, *Cd36*, *Ftar2*, *Prdm1* and *Aqp3*) did not validate in the peripheral organs (spleen and pLNs) and were therefore discarded from the final signature panel. Third, all 13 γδ^{IFN}-biased genes were validated in the spleen and pLNs, thus making the cut as γδ^{IFN} signature genes. Fourth, 10 of the 13 γδ^{IFN} signature genes were not differentially expressed in thymocyte subsets but only segregated in peripheral lymphoid organs after being switched off in γδ^{17} cells. Fifth, many of the validated genes (both γδ^{17} and γδ^{IFN} cell signatures) were increased in expression between the thymus and periphery (Fig. 4a,b). These data strongly suggest a progressive differentiation process (or 'adaptation') following thymic export underlying the large segregation of the peripheral γδ^{17} versus γδ^{IFN} transcriptomes (Fig. 1e–i). Importantly, as an outcome of these comprehensive analyses, we provide the community with a panel of 20 new validated γδ^{17}/γδ^{IFN} cell signature genes for future study of their distinct functions in pathophysiology (Table 1). To exclude a major influence of PMA/ionomycin stimulation (used to induce reporter activity) on these expression patterns, we sorted CD44^{high}CD45RB$^-$ and CD45RB$^+$CD44$^+$ γδ T cells from the pLNs of C57BL/6 mice, which enrich for IL-17 or IFNγ producers, respectively[10] (Extended Data Fig. 1d). Importantly, we found that the vast majority (16 of 20) of signature genes showed differential expression patterns in these ex vivo γδ T cell subsets from pLNs (Extended Data Fig. 4). We also analyzed equivalent subsets isolated from the liver, which is naturally enriched in γδ^{IFN} cells[3], and from the testes, which harbor a major tissue-resident γδ^{17} cell population[13]. We did not find a consistent trend for up- or downregulation of gene expression between pLNs and these other tissues, although some γδ^{17} cell signature genes (*Dgat1*, *Ptgs2* and *Ret*) were enriched in the testis. As for γδ^{IFN} cell signatures, we observed that seven were augmented, whereas four were reduced in liver CD45RB$^+$CD44$^+$ γδ T cells (compared with other tissues). The latter included three of four genes associated with TCR signaling (*Themis*, *Cd6* and *Slamf6*; Extended Data Fig. 4).

To test the robustness of our approach in resolving the transcriptomes of γδ^{17} and γδ^{IFN} cells, we compared the differential pattern of expression of our 20 validated signature genes in γδ17 and γδ^{IFN} cells from two publicly available single-cell RNA-seq datasets of LN γδ T cells by Yang et al.[14] and du Halgouet et al.[15]. Interestingly, some signature genes were either not detected or failed to be differentially expressed between γδ^{17} and γδ^{IFN} cells in those studies (Extended Data Fig. 5),

https://doi.org/10.1038/s41590-024-02073-8

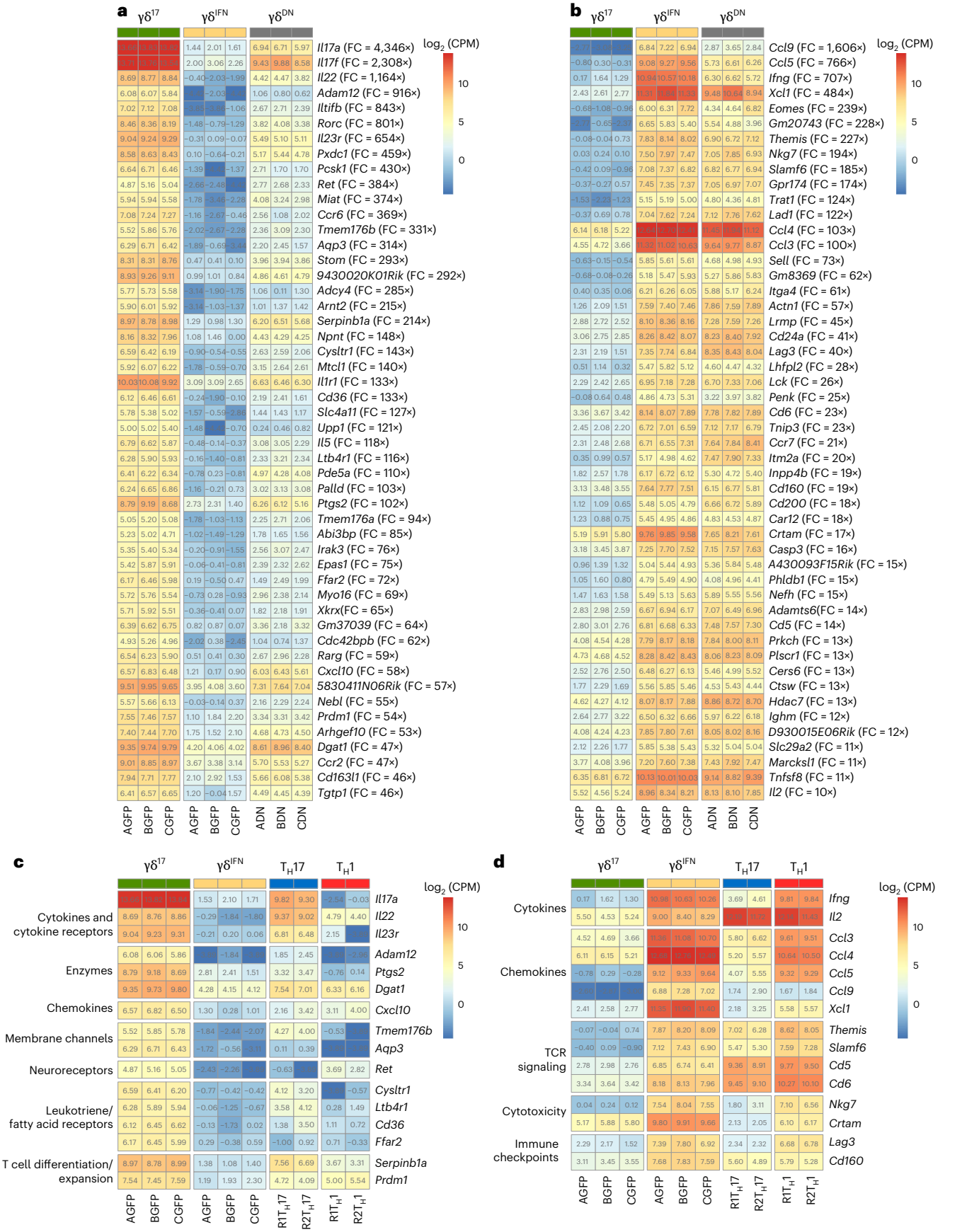

Fig. 3 | Identification of signature genes in peripheral γδ^{17} versus γδ^{IFN} cells. **a**,**b**,Heat maps displaying the $\log_2$ (CPM) normalized expression values of the 50 most enriched differentially expressed genes in γδ^{17} cells (**a**) and the 50 most enriched genes in γδ^{IFN} cells (**b**), ordered by fold change, in γδ^{17}, γδ^{IFN} and γδ^{DN} cells. **c**,**d**, Heat maps displaying the $\log_2$ (CPM) normalized expression values of selected candidates (CPM > 30 with known biological function) enriched in γδ^{17} (**c**) and γδ^{IFN} (**d**) cells, manually grouped by functional categories, in γδ^{17}, γδ^{IFN}, T_H17 and T_H1 cells.

https://doi.org/10.1038/s41590-024-02073-8

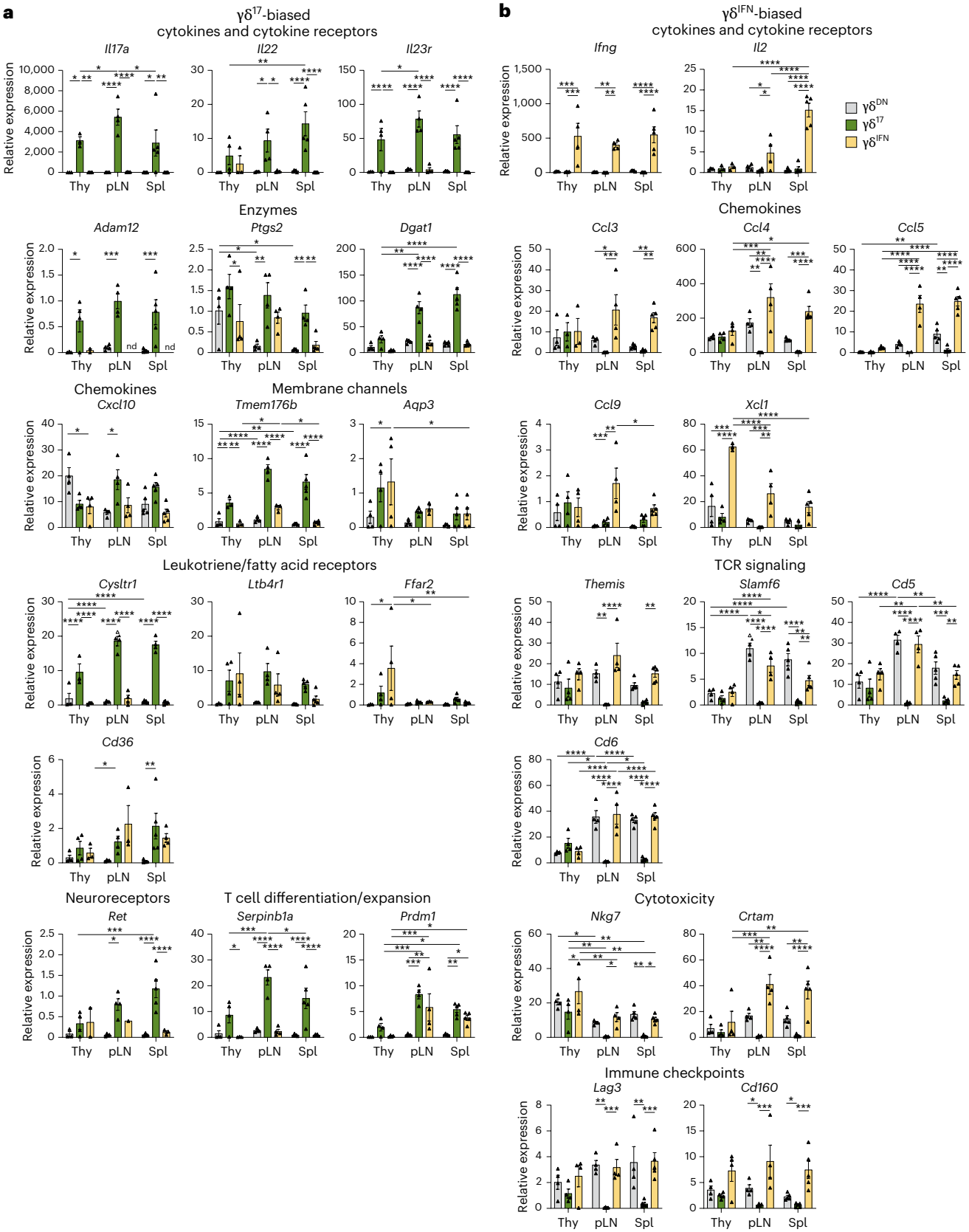

Fig. 4 | Patterns of expression of γδ^{17} versus γδ^{IFN} signature genes across lymphoid organs. a,**b**, γδ^{DN} (GFP^{-}YFP^{-}), γδ^{17} (GFP^{+}) and γδ^{IFN} (YFP^{+}) γδ T cells were sorted, and RNA was extracted and subjected to RT–qPCR analysis. Relative expression levels of γδ^{17} cell signature genes (**a**) and γδ^{IFN} cell signature genes (**b**) were normalized to that of *Actb* (β-actin); nd, not detected; Thy, thymus; Spl, spleen. Data are representative of one to four independent experiments. Each symbol indicates a pool of cells from several mice. Data are shown as mean ± s.e.m. and were analyzed by one-way analysis of variance (ANOVA) with a Tukey's multiple comparisons test under the assumption of data normality; $^{*}P \leq 0.05$, $^{**}P \leq 0.01$, $^{***}P \leq 0.001$ and $^{****}P \leq 0.0001$.

https://doi.org/10.1038/s41590-024-02073-8

Table 1 | Panel of validated signature genes in peripheral γδ^{17} versus γδ^{IFN} cells

γδ^{17} signature	Function	γδ^{IFN} signature	Function
Adam12, Ptgs2, Dgat1	Enzymes	*Ccl3, Ccl4, Ccl5, Ccl9, Xcl1*	Chemokines
Ret	Neuroreceptors	*Themis, Slamf6, Cd5, Cd6*	TCR signaling
Tmem176b	Membrane channels	*Nkg7, Crtam*	Cytotoxicity
Cysltr1	Leukotriene receptors	*Lag3, Cd160*	Immune checkpoints
Serpinb1a	T cell expansion		

Selected differentially expressed genes from RNA-seq analysis (Fig. 3) that were validated by RT–qPCR in independent samples of peripheral γδ^{17} versus γδ^{IFN} cells (Fig. 4).

whereas others, despite showing the same trend, exhibited a much lower fold change than our data (Extended Data Fig. 5c,d). This highlights the added value of the increased depth of bulk RNA-seq of pure effector γδ T cell subsets to specifically resolve their transcriptomes.

Next, we asked if the expression pattern of the γδ^{17}/γδ^{IFN} signature genes would be maintained under pathophysiological conditions. To address this, we analyzed our gene panel in sorted reporter-based γδ T cell subsets isolated from two disease models in which γδ^{17} or γδ^{IFN} responses have been shown to be functionally important: EAE[16] and ECM induced with *P. berghei* ANKA sporozoites[3,4]. In EAE, where γδ^{17} cells are involved[16], we found all (except *Ptgs2*) γδ^{17} signature genes to maintain their differential expression pattern, whereas several TCR-associated genes among γδ^{IFN} signature genes were seemingly downregulated in γδ^{IFN} cells (Fig. 5). However, in the ECM model, where γδ^{IFN} cells are most relevant[3], they maintained the selective enrichment in most γδ^{IFN} signatures, whereas γδ^{17} signature genes were more highly expressed in γδ^{17} cells (Fig. 6). These data attest to the utility of our γδ^{17}/γδ^{IFN} signature gene panel to characterize effector γδ T cells under pathophysiological conditions.

CD6 and Themis are regulators of γδ^{IFN} cell activation

Finally, we aimed at proof-of-concept functional validation of some γδ^{17}/γδ^{IFN} signature genes. Based on our focus on the peripheral functions of these subsets, we considered potential regulators of their activation. Although these were not obvious among the γδ^{17} signatures, two γδ^{IFN}-biased genes seemed particularly attractive given their association with TCR signaling: *Cd6* and *Themis* (Table 1). CD6 is a T cell-specific membrane glycoprotein that physically colocalizes and associates with the TCR–CD3 complex and participates as a 'co-receptor' in the activation of αβ T cells[17], but its role in γδ T cells remains poorly understood[18]. Similarly, Themis is also a T cell-specific protein with important roles in αβ T cell development and activation, namely promoting thymocyte positive selection[19–21] and CD8$^+$ T cell proliferative responses to low-affinity ligands[22] but which, to our knowledge, has never been studied in γδ T cells.

We validated the differential expression of CD6 and Themis, previously observed by RNA-seq (Fig. 3c,d) and RT–qPCR (Fig. 4b and Extended Data Fig. 4b), in γδ^{17} versus γδ^{IFN} cells from *Il17a*-GFP:*Ifng*-YFP mice at the level of surface and intracellular protein expression by flow cytometry analysis of C57BL/6 mouse γδ T cell subsets (Fig. 7a,b). These cell subsets were defined according to CD44 and CD45RB expression (as in Extended Data Fig. 1c): mature (CD24$^-$) γδ T cells with a CD44^{high}CD45RB$^-$ phenotype contain γδ^{17} cells, whereas γδ^{IFN} cells are enriched within CD44$^+$CD45RB$^+$ cells, and 'naive' cells remain CD44$^-$CD45RB$^-$, as previously reported[10]. We found both proteins to be selectively absent from peripheral CD24$^-$CD44^{high}CD45RB$^-$ cells (Fig. 7a,b), consistent with the downregulation of *Cd6* and *Themis* mRNA expression in γδ^{17} cells between the thymus and peripheral lymphoid organs (Fig. 4b). Furthermore, we found normal numbers of total γδ thymocytes and similar (to wild-type (WT) control mice) frequencies of Vγ- or CD44/CD45RB-based subsets as well as IL-17$^+$ or IFNγ$^+$ γδ thymocytes in specific loss-of-function models: *Cd6*$^{Δd3/Δd3}$-mutant mice, where the critical domain 3 of CD6 was ablated to prevent interaction with its ligand CD166 (ref. 23), and *Themis*-knockout (*Themis*-KO) mice[19] (Extended Data Fig. 6).

Based on these data, we postulated that both CD6 and Themis might impact the peripheral activation of γδ^{IFN} cells as well as 'naive' γδ T cells, which are collectively marked by CD27 expression (unlike γδ^{17} cells that lack CD27 expression)[24]. To test this hypothesis, we analyzed the response to in vitro and in vivo stimulation of CD27$^+$ γδ T cells isolated from *Cd6*$^{Δd3/Δd3}$-mutant and *Themis*-KO mice compared with respective littermate controls. Importantly, because both proteins are T cell specific, only this lineage is directly impacted in these models. First, we assessed the expression of T cell activation-associated markers (CD44, CD69 and CD25) in CellTrace Violet (CTV)-labeled CD27$^+$ γδ T cells sorted by FACS from pooled pLNs and spleen tissue after 72 h of in vitro stimulation. We used two experimental setups. For CD6, because its normal function requires surface interaction with CD166 expressed on antigen-presenting cells, we provided these as T cell-depleted splenocytes plus increasing concentrations of soluble monoclonal anti-CD3. For Themis, being an intracellular protein, we simply cultured the cells with plate-bound monoclonal anti-CD3 and anti-CD28. *Cd6*$^{Δd3/Δd3}$-mutant and especially Themis-deficient CD27$^+$ γδ T cells exhibited lower expression frequencies of these surface markers, indicating an impaired activation status compared with their respective WT littermates (Fig. 7c,d). Furthermore, following analysis of CTV dilution as a measure of cell proliferation, we found an impact at lower to intermediate TCR agonist (erased at saturating 2.5 μg ml^{-1} monoclonal anti-CD3) concentrations, which was particularly striking for *Themis*-KO mice (Fig. 7e–h). By contrast, the activation and proliferation of γδ^{17}-biased CD27$^-$ γδ T cells from both *Cd6*$^{Δd3/Δd3}$-mutant and Themis-deficient mice was comparable to WT control mice, showing the selectivity for γδ^{IFN}-biased cells (Extended Data Fig. 7).

To assess the relevance of these findings in an in vivo setting, we again used the ECM model, given the key role of γδ^{IFN} cells in this disease and their increase in activation status, proliferation and effector functions, leading to an IFNγ-dependent inflammatory response that becomes fatal at 7–8 days postinfection[3,4,25]. Interestingly, both *Cd6*$^{Δd3/Δd3}$-mutant mice and *Themis*-KO mice were much less susceptible than control littermates to ECM (Fig. 7i,j). Of note, no significant differences were found in parasitemia levels (Fig. 7i,j), thus excluding parasite load as the cause for the observed phenotypes, similar to what we found in mice selectively deficient in γδ^{IFN} cells[4,25]. Importantly, the ECM phenotypes associated with differences in γδ^{IFN} cell activation and proliferation were more substantial for *Themis*-KO than for *Cd6*$^{Δd3/Δd3}$-mutant mice (Fig. 7k–n).

Collectively, these results establish CD6 and especially Themis as regulators of peripheral γδ^{IFN} cell activation in vitro and in vivo, thus attesting the functional relevance of our study.

Discussion

The immunological roles of γδ^{17} and γδ^{IFN} cell subsets have been previously demonstrated in multiple infection, inflammation and cancer models[1,2]. In this study, we dissected the biological differences between LN γδ^{17} versus γδ^{IFN} cells isolated from *Il17a*-GFP:*Ifng*-YFP mice that faithfully reported the expression of the signature cytokines produced by these subsets. This constitutes an advance relative to previous studies that used cell surface[26] markers to enrich for γδ^{17} and γδ^{IFN} cells but that could not avoid contamination with non-effector γδ T cells (as illustrated in Extended Data Fig. 1b). Furthermore, cytokine transcripts are notoriously poorly detected using single-cell RNA-seq analyses, making us opt for a bulk RNA-seq strategy using reporter mice instead of a single-cell strategy, like in previous studies[26–28,15], to achieve maximal depth of analysis of the transcriptomes directly associated with the

https://doi.org/10.1038/s41590-024-02073-8

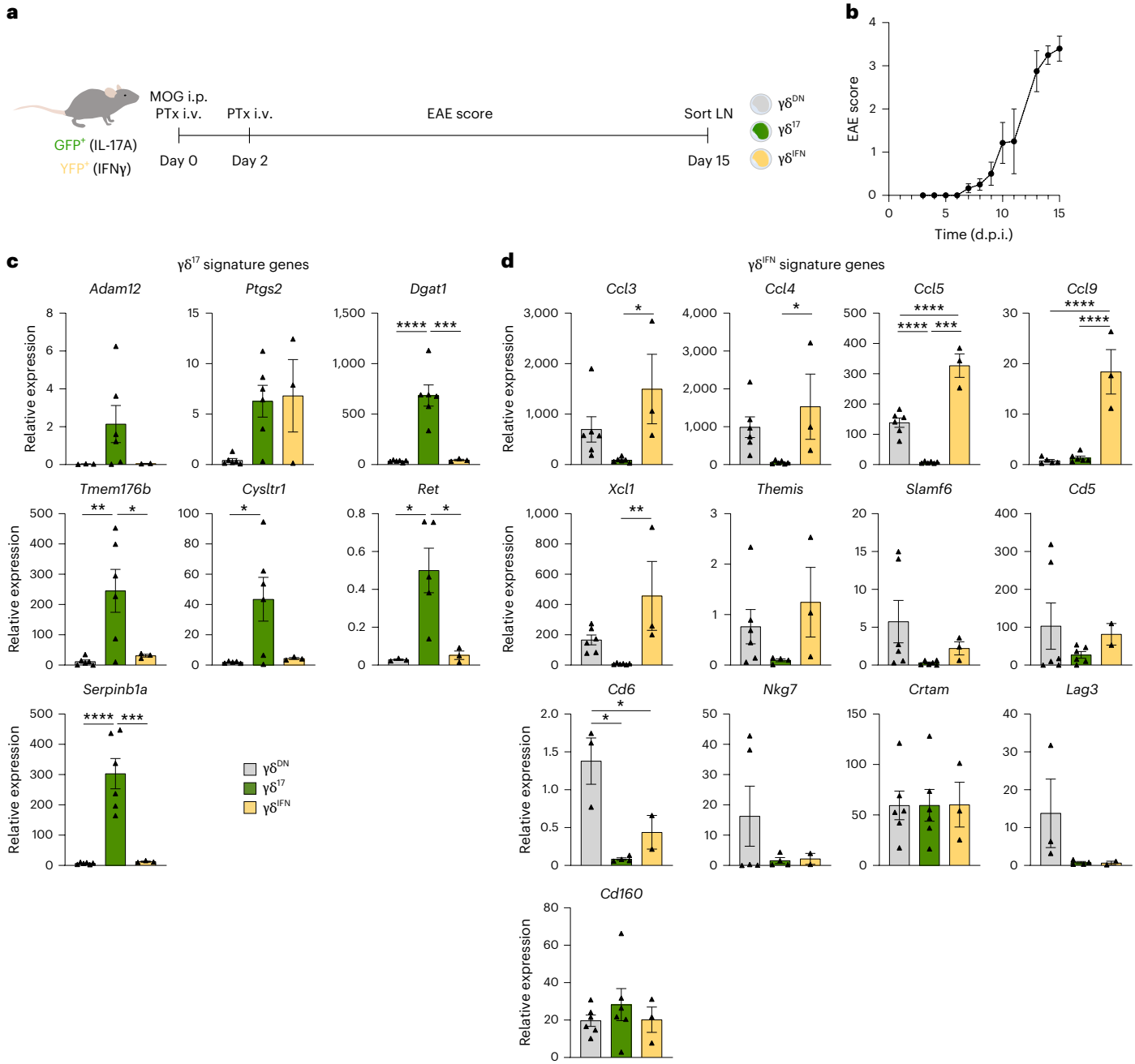

Fig. 5 | Expression of signature genes in γδ^{17} and γδ^{IFN} cells in EAE induction. **a**, Schematic representation of the experimental design. Double *Il17a*-GFP:*Ifng*-YFP reporter mice were subjected to EAE, and γδ^{DN} (GFP$^-$YFP$^-$), γδ^{17} (GFP$^+$) and γδ^{IFN} (YFP$^+$) cells from pLNs were isolated by FACS at the peak plateau stage (day 15) to perform RNA extraction, followed by RT–qPCR analysis; MOG, myelin oligodendrocyte glycoprotein; i.p., intraperitoneal; i.v., intravenous; PTx, pertussis toxin. **b**, EAE clinical score of *Il17a*-GFP:*Ifng*-YFP reporter mice ($n = 8$) until 15 days postimmunization (d.p.i.). **c**,**d**, Relative expression levels of validated γδ^{17} signature genes (**c**) and γδ^{IFN} signature genes (**d**) were normalized to *Actb* (β-actin). Data are representative of two to six independent experiments. Each symbol represents a pool of cells from several mice. Data are shown as mean ± s.e.m. and were analyzed by one-way ANOVA with a Tukey's multiple comparisons test under the assumption of data normality; $^*P \le 0.05$, $^{**}P \le 0.01$, $^{***}P \le 0.001$ and $^{****}P \le 0.0001$.

expression of signature cytokines. This allowed us to obtain approximately 40 million reads for each γδ T cell subset, which constitutes an over 100-fold increase in depth relative to the previous studies by Yang et al.[14] and du Halgouet et al.[15].

An unanticipated finding from our genome-wide RNA-seq analysis was that 49% of all the >12,800 genes expressed in γδ T cells were differentially expressed between γδ^{17} and γδ^{IFN} cell subsets. In fact, looking at the segregation of expressed genes across the three sequenced populations, it was clear that the transcriptome of γδ^{17} cells diverged not only from that of γδ^{IFN} cells but also from γδ^{DN} cells. This may be due to an early γδ^{17} cell 'lineage split' during thymic γδ T cell development, given that Kang and colleagues have identified a SOX13$^+$ DN1 thymocyte progenitor population that generates γδ^{17} but not γδ^{IFN} cells along a TCR-independent pathway[29]. By contrast, the development of γδ^{IFN} thymocytes is known to be promoted by strong, likely ligand-dependent, TCR signaling[10,25,29–31]. In that regard, the presence of 10–15% γδ^{IFN} cells in naive (unchallenged) mice may suggest their self-reactivity based on thymic ligand encounter[30], consistent with the observed expression of gene signatures associated with TCR signaling. Our data also suggest that this distinct involvement of TCR signaling extends from

https://doi.org/10.1038/s41590-024-02073-8

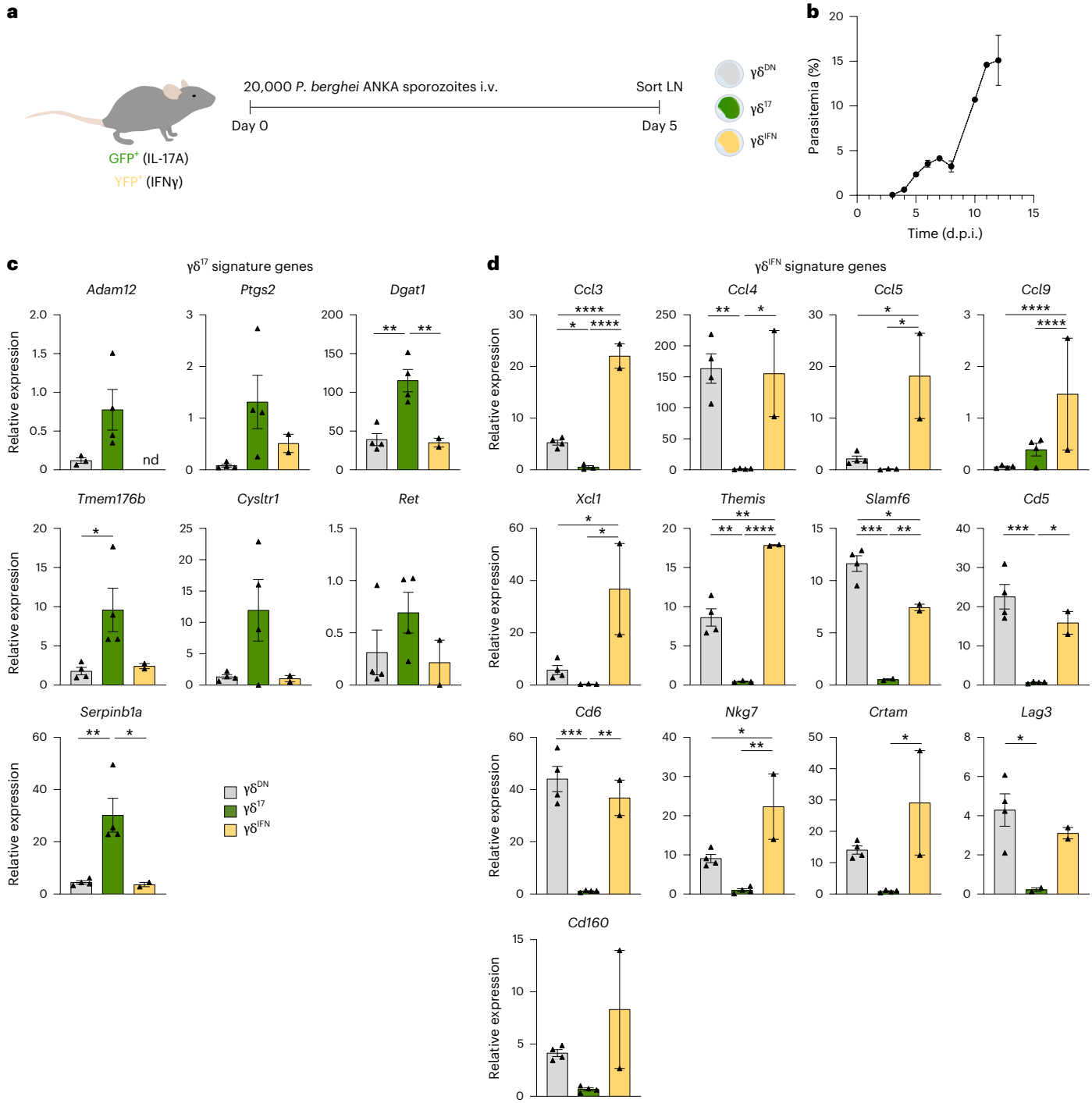

Fig. 6 | Expression of signature genes in γδ^{17} and γδ^{IFN} cells following malaria infection. a, Schematic representation of the experimental design. Double *Il17a*-GFP:*Ifng*-YFP reporter mice were infected with 2×10^4 *P. berghei* ANKA GFP sporozoites via retro-orbital injection, and γδ^{DN} (GFP$^-$YFP$^-$), γδ^{17} (GFP$^+$) and γδ^{IFN} (YFP$^+$) cells from pLNs were isolated by FACS at day 5 postinfection. **b**, Parasitemia of infected *Il17a*-GFP:*Ifng*-YFP reporter mice in days postinfection ($n = 11$). **c**,**d**, Relative expression levels of validated γδ^{17} signature genes (**c**) and γδ^{IFN} signature genes (**d**) were normalized to *B2m* (β_2-microglobulin). Data are representative of two to four independent experiments. Each symbol represents a pool of cells from several mice. Data are shown as mean ± s.e.m. and were analyzed by one-way ANOVA with a Tukey's multiple comparisons test under the assumption of data normality; $^*P \le 0.05$, $^{**}P \le 0.01$, $^{***}P \le 0.001$ and $^{****}P \le 0.0001$.

the thymus to the periphery because a gene module associated with TCR signaling (including *Cd6* and *Themis*) was selectively upregulated in LN γδ^{IFN} cells compared with in γδ^{17} cells (Fig. 3d). These results are consistent with previous observations of the high responsiveness of peripheral γδ^{IFN} (but not γδ^{17}) cells to direct TCR stimulation, whereas γδ^{17} cells preferentially respond to innate signals such as IL-1β and IL-23 (refs. 16,32). In fact, our data indicate a broad capacity of peripheral γδ^{17} cells to sense the environment, as they were highly enriched in KEGG pathways related to environmental information processing and modules of the endocrine and nervous systems (Supplementary Table 5), which opens exciting avenues for research.

Our γδ^{17}/γδ^{IFN} cell signature 20-gene panel (Table 1) was derived from the top 50 differentially expressed genes (in the RNA-seq analysis) between the two subsets on the basis of their known biological function

https://doi.org/10.1038/s41590-024-02073-8

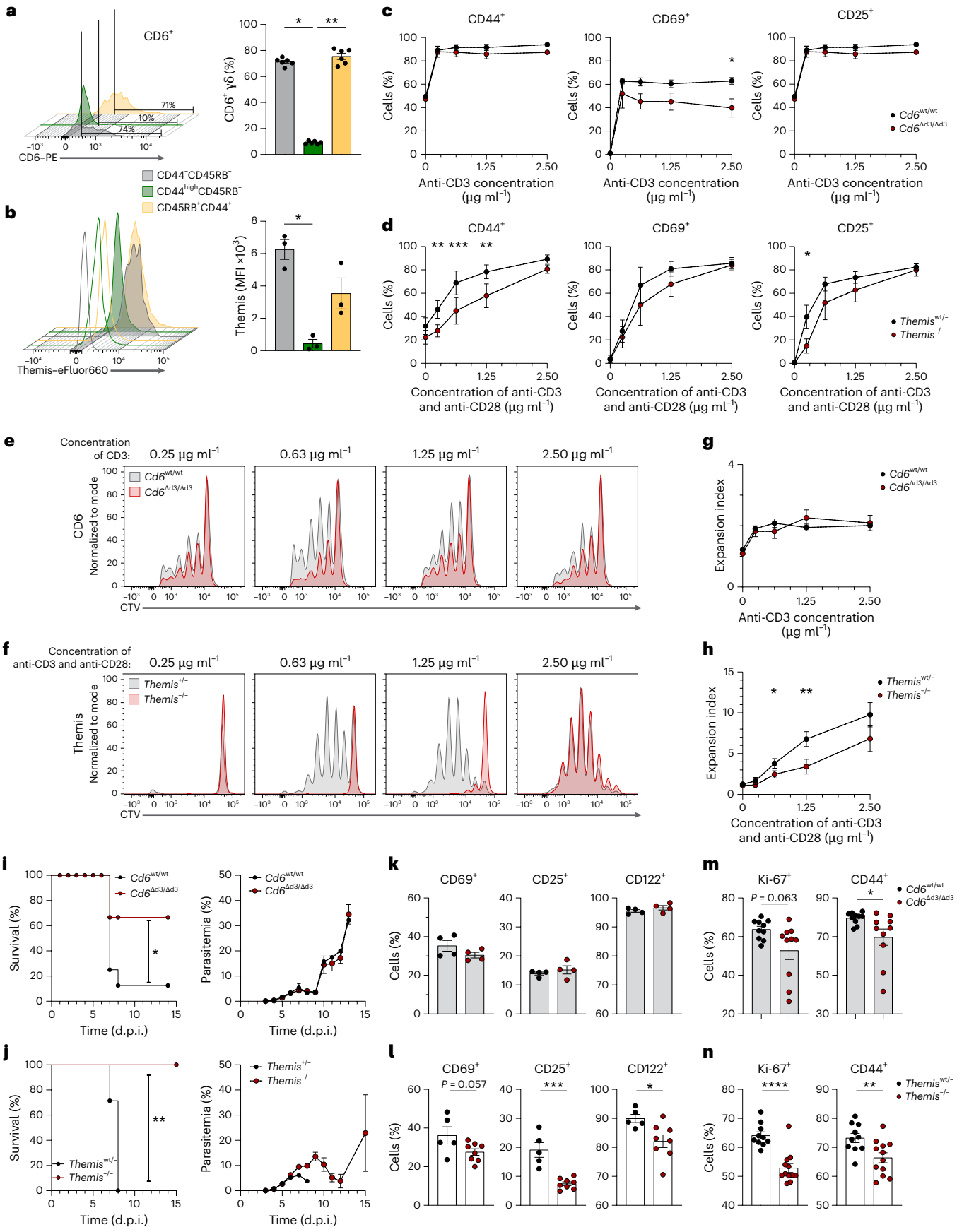

Fig. 7 | CD6 and Themis promote the activation and proliferation of peripheral CD27$^+$ γδ^{IFN}-biased cells. a,**b**, Flow cytometry analyses of the frequency of CD6$^+$ cells within CD44$^-$CD45RB$^-$, CD44^{high}CD45RB$^-$ and CD45RB$^+$CD44$^+$ γδ T cell subsets from the pLNs of C57BL/6 mice (data are representative of two independent experiments; $n = 6$; **a**) or mean fluorescence intensity (MFI) of Themis (**b**) within those subsets from the pLNs of *Themis*$^{+/-}$ (filled histograms) and *Themis*$^{-/-}$ mice (empty histograms). In the MFI summary graph, each symbol corresponds to the subtraction of the autofluorescence from each subset in *Themis*$^{-/-}$ mice to that of the respective *Themis*$^{+/-}$ control (data are representative of three independent experiments; $n = 3$). **c**,**d**, Frequencies of CD44 or CD69 (at 48 h) and CD25 (at 72 h) expression in CTV-labeled CD27$^+$ γδ T cells from the pLNs and spleens of *Cd6*$^{\Delta d3/\Delta d3}$ and control mice stimulated for 72 h with increasing concentrations of soluble anti-CD3 in the presence of T cell-depleted splenocytes (data are representative of three independent experiments; $n = 3$; each replicate constitutes a pool of three mice; **c**) or *Themis*$^{-/-}$ and control mice after 72 h of stimulation with increasing concentrations of plate-bound monoclonal anti-CD3 plus anti-CD28 (data are representative of five ($n = 5$, 48 h) or eight ($n = 8$, 72 h) independent experiments; each replicate constitutes a pool of two mice). **e**–**h**, Representative plots of CTV dilution at 72 h of proliferating CD27$^+$ γδ T cells from *Cd6*$^{\Delta d3/\Delta d3}$ (**e**) or *Themis*$^{-/-}$ (**f**) and control mice in the aforementioned culture systems (**c** and **d**) as well as respective expansion indexes for CD6 ($n = 3$; **g**) and Themis ($n = 8$; **h**). **i**,**j**, Survival (left) and parasitemia (right) of *Cd6*$^{\Delta d3/\Delta d3}$ and control mice ($n = 11$; **i**) and *Themis*$^{-/-}$ and control mice (survival $n = 7$, parasitemia $n = 14$; **j**) infected with *P. berghei* ANKA GFP sporozoites. Data are representative of two independent experiments. **k**,**l**, Frequencies of CD69, CD25 and CD122 expression in γδ^{IFN}-committed CD45RB$^+$CD44$^+$ cells from the pLNs of infected *Cd6*$^{\Delta d3/\Delta d3}$ ($n = 4$) and control ($n = 4$) mice (**k**) and *Themis*$^{-/-}$ ($n = 8$) and control ($n = 5$) mice (**l**) 5 days postinfection. Data are from one (*Cd6*) or two (*Themis*) independent experiments. **m**,**n**, Frequencies of Ki-67 and CD44 in IFNγ$^+$ γδ T cells from the pLNs of infected *Cd6*$^{\Delta d3/\Delta d3}$ ($n = 10$) and control ($n = 10$) mice (**m**) and *Themis*$^{-/-}$ ($n = 12$) and control ($n = 10$) mice (**n**). Data are from three independent experiments and are shown as mean ± s.e.m. Data were analyzed by Kruskal–Wallis test (**a** and **b**) or two-way ANOVA (**c** and **d**) and mixed effects model (**g** and **h**), under the assumption of data normality, for multiple comparisons. Survival data were analyzed by log-rank test (**i** and **j**), and single comparisons were analyzed by Mann–Whitney or *t*-test (**k** and **n**); $^*P \le 0.05$, $^{**}P \le 0.01$, $^{***}P \le 0.001$ and $^{****}P \le 0.0001$.

and validation (in independent LN and spleen samples) by RT–qPCR (Fig. 4). Interestingly, these genes were generally not differentially expressed between T_H17 and T_H1 cells (Extended Data Fig. 2d,e) based on a unique comparison that took advantage of parallel ex vivo RNA-seq analyses of populations isolated from our double-reporter mice. Globally, this comparison revealed a much higher number of genes that were differentially expressed between γδ^{17} and γδ^{IFN} cells than between T_H17 and T_H1 cells (Extended Data Fig. 2b,c), further illustrating the striking transcriptome divergence among effector γδ T cell subsets.

The validated γδ^{17}/γδ^{IFN} cell signature panel is composed of 7 γδ^{17}-biased and 13 γδ^{IFN}-enriched genes (Table 1). They reflect important functional attributes of the two subsets. For example, on the γδ^{17} side, RET is a neuroreceptor tyrosine kinase that controls IL-22 production by innate lymphoid cells[33], ADAM12 is a cancer-associated sheddase implicated in the release of ligands that promote the formation and progression of tumors[34], and *Ptgs2* encodes the COX-2 enzyme that produces prostaglandin E_2, which orchestrates tumor-promoting inflammation[35]. Among γδ^{IFN} cell-enriched genes, we notably found the chemokines CCL3, CCL4, CCL5, CCL9 and XCL1, which, together with CCL1, have been shown to characterize pathogen-specific effector αβ T cells in multiple in vivo challenges[36]; NKG7, a regulator of lymphocyte granule exocytosis and cytotoxicity in infection and cancer[37], and LAG-3, an immune checkpoint receptor protein found on the surface of activated T cells that is being actively explored for cancer immunotherapy[38]. Although all these γδ^{17}/γδ^{IFN} signature genes will certainly be interesting to explore at the functional level in effector γδ T cell subsets, here, we focused on two other γδ^{IFN}-biased genes, which we hypothesized to regulate peripheral γδ^{IFN} cell activation: *Cd6* and *Themis*.

Although CD6 and Themis have been both implicated in modulating TCRαβ signaling, the underlying mechanisms remain controversial. For the surface co-receptor CD6, both stimulatory and inhibitory roles have been proposed in αβ T cell activation, likely due to differential involvement of its various extracellular and intracellular domains[17,39,40]. Indeed, within the CD6 cytosolic interactome, a delicate equilibrium of activating and inhibitory effectors seemingly orchestrates context-dependent responses[41]. Notably, the interaction with CD166, regulated by alternative splicing-mediated inclusion or skipping of the ligand-binding domain (d3)[42], influences the strength of cell adhesion during T cell activation[43]. Similarly, the intracellular protein Themis has been associated during αβ thymocyte development with either enhancing[21,44,45] or reducing[46] TCRαβ signaling in response to low-affinity peptide–major histocompatibility complex ligands. As for peripheral αβ T cells, CD8$^+$ T cells seemingly rely on Themis for their maintenance and proliferation in response to homeostatic cytokines such as IL-2 and IL-15 (refs. 22,47). CD4$^+$ T cells increased Themis expression specifically during T_H1 differentiation, which contributed to their IFNγ-based response in a mouse model of multiple sclerosis[48].

We now show in γδ T cells that both *Cd6* and *Themis* specifically promote the in vitro activation and expansion of γδ^{IFN} cells, or, more broadly, γδ^{IFN}-biased CD27$^+$ γδ cells (Fig. 7), and not γδ^{17}-biased CD27$^-$ γδ cells (Extended Data Fig. 7), as both genes are effectively shut down in peripheral γδ^{17} cells (Fig. 4b), in stark contrast to T_H17 cells (Fig. 3d). Interestingly, we did not find any thymic γδ T cell phenotypes in either *Cd6*$^{\Delta d3/\Delta d3}$-mutant or *Themis*-KO mice (Extended Data Fig. 6), which clearly places these molecules as regulators of the activation of peripheral γδ^{IFN}-biased cells. This concept was validated in ECM following *P. berghei* sporozoite infection, a model in which γδ^{IFN} cells act upstream of αβ T cell responses to drive disease pathogenesis[3]. It may also be relevant for other pathophysiological settings where γδ^{IFN} cells have been implicated[1,2]. However, building on the ECM data, it will be interesting to consider CD6 and Themis expression and potential modulation in human γδ T cells following *Plasmodium* infection, given their importance both in protective responses and in the pathogenesis of severe malaria[49].

In summary, this study provides a detailed transcriptomic analysis of bona fide γδ^{17} and γδ^{IFN} cell subsets, which unveiled differentially expressed genes that had not been reported before, including a panel of 20 signature genes validated in various tissues at steady-state and following EAE and ECM challenge, highlighting its potential to characterize γδ T cells in preclinical models and likely also in human disease.

Online content

Any methods, additional references, Nature Portfolio reporting summaries, source data, extended data, supplementary information, acknowledgements, peer review information; details of author contributions and competing interests; and statements of data and code availability are available at https://doi.org/10.1038/s41590-024-02073-8.

References

1. Ribot, J. C., Lopes, N. & Silva-Santos, B. γδ T cells in tissue physiology and surveillance. *Nat. Rev. Immunol.* **21**, 221–232 (2021).
2. Silva-Santos, B., Mensurado, S. & Coffelt, S. B. γδ T cells: pleiotropic immune effectors with therapeutic potential in cancer. *Nat. Rev. Cancer* **19**, 392–404 (2019).
3. Ribot, J. C. et al. γδ-T cells promote IFN-γ-dependent *Plasmodium* pathogenesis upon liver-stage infection. *Proc. Natl Acad. Sci. USA* **116**, 9979–9988 (2019).

4. Chora, A. F. et al. Interplay between liver and blood stages of *Plasmodium* infection dictates malaria severity via γδ T cells and IL-17-promoted stress erythropoiesis. *Immunity* **56**, 592–605 (2023).
5. Fiala, G. J., Gomes, A. Q. & Silva-Santos, B. From thymus to periphery: molecular basis of effector γδ-T cell differentiation. *Immunol. Rev.* **298**, 47–60 (2020).
6. Haas, J. D. et al. Development of interleukin-17-producing γδ T cells is restricted to a functional embryonic wave. *Immunity* **37**, 48–59 (2012).
7. Edwards, S. C. et al. PD-1 and TIM-3 differentially regulate subsets of mouse IL-17A-producing γδ Tcells. *J. Exp. Med.* **220**, e20211431 (2023).
8. Narayan, K. et al. Intrathymic programming of effector fates in three molecularly distinct γδ T cell subtypes. *Nat. Immunol.* **13**, 511–518 (2012).
9. Schmolka, N. et al. Epigenetic and transcriptional signatures of stable versus plastic differentiation of proinflammatory γδ T cell subsets. *Nat. Immunol.* **14**, 1093–1100 (2013).
10. Sumaria, N., Grandjean, C. L., Silva-Santos, B. & Pennington, D. J. Strong TCRγδ signaling prohibits thymic development of IL-17A-secreting γδ T cells. *Cell Rep.* **19**, 2469–2476 (2017).
11. Codarri, L. et al. RORγt drives production of the cytokine GM-CSF in helper T cells, which is essential for the effector phase of autoimmune neuroinflammation. *Nat. Immunol.* **12**, 560–567 (2011).
12. Carding, S. R. & Egan, P. J. γδ T cells: functional plasticity and heterogeneity. *Nat. Rev. Immunol.* **2**, 336–345 (2002).
13. Wilharm, A. et al. Microbiota-dependent expansion of testicular IL-17-producing Vγ6$^+$ γδ T cells upon puberty promotes local tissue immune surveillance. *Mucosal Immunol.* **14**, 242–252 (2021).
14. Yang, T. et al. RORγt$^+$ c-Maf$^+$ Vγ4$^+$ γδ T cells are generated in the adult thymus but do not reach the periphery. *Cell Rep.* **42**, 113230 (2023).
15. du Halgouet, A. et al. Multimodal profiling reveals site-specific adaptation and tissue residency hallmarks of γδ T cells across organs in mice. *Nat. Immunol.* **25**, 343–356 (2024).
16. Sutton, C. E. et al. Interleukin-1 and IL-23 induce innate IL-17 production from γδ T cells, amplifying T_H17 responses and autoimmunity. *Immunity* **31**, 331–341 (2009).
17. Gimferrer, I. et al. Relevance of CD6-mediated interactions in T cell activation and proliferation. *J. Immunol.* **173**, 2262–2270 (2004).
18. Pawelec, G. & Buhring, H. J. Monoclonal antibodies to CD6 preferentially stimulate T-cell clones with γ/δ rather than α/β antigen receptors. *Hum. Immunol.* **31**, 165–169 (1991).
19. Lesourne, R. et al. Themis, a T cell-specific protein important for late thymocyte development. *Nat. Immunol.* **10**, 840–847 (2009).
20. Fu, G. et al. Themis controls thymocyte selection through regulation of T cell antigen receptor-mediated signaling. *Nat. Immunol.* **10**, 848–856 (2009).
21. Choi, S. et al. THEMIS enhances TCR signaling and enables positive selection by selective inhibition of the phosphatase SHP-1. *Nat. Immunol.* **18**, 433–441 (2017).
22. Brzostek, J. et al. T cell receptor and cytokine signal integration in CD8$^+$ T cells is mediated by the protein Themis. *Nat. Immunol.* **21**, 186–198 (2020).
23. Santos, R. F., Oliveira, L., Brown, M. H. & Carmo, A. M. Domain-specific CD6 monoclonal antibodies identify CD6 isoforms generated by alternative-splicing. *Immunology* **157**, 296–303 (2019).
24. Ribot, J. C. et al. CD27 is a thymic determinant of the balance between interferon-γ- and interleukin 17-producing γδ T cell subsets. *Nat. Immunol.* **10**, 427–436 (2009).
25. Munoz-Ruiz, M. et al. TCR signal strength controls thymic differentiation of discrete proinflammatory γδ T cell subsets. *Nat. Immunol.* **17**, 721–727 (2016).
26. Tan, L. et al. Single-cell transcriptomics identifies the adaptation of Scart1$^+$ Vγ6$^+$ T cells to skin residency as activated effector cells. *Cell Rep.* **27**, 3657–3671 (2019).
27. Sagar et al. Deciphering the regulatory landscape of fetal and adult γδ T-cell development at single-cell resolution. *EMBO J.* **39**, e104159 (2020).
28. Sanchez Sanchez, G. et al. Identification of distinct functional thymic programming of fetal and pediatric human γδ thymocytes via single-cell analysis. *Nat. Commun.* **13**, 5842 (2022).
29. Spidale, N. A. et al. Interleukin-17-producing γδ T cells originate from SOX13$^+$ progenitors that are independent of γδTCR signaling. *Immunity* **49**, 857–872 (2018).
30. Jensen, K. D. et al. Thymic selection determines γδ T cell effector fate: antigen-naive cells make interleukin-17 and antigen-experienced cells make interferon-γ. *Immunity* **29**, 90–100 (2008).
31. Turchinovich, G. & Hayday, A. C. Skint-1 identifies a common molecular mechanism for the development of interferon-γ-secreting versus interleukin-17-secreting γδ T cells. *Immunity* **35**, 59–68 (2011).
32. Ribot, J. C. et al. Cutting edge: adaptive versus innate receptor signals selectively control the pool sizes of murine IFN-γ- or IL-17-producing γδ T cells upon infection. *J. Immunol.* **185**, 6421–6425 (2010).
33. Ibiza, S. et al. Glial-cell-derived neuroregulators control type 3 innate lymphoid cells and gut defence. *Nature* **535**, 440–443 (2016).
34. Duffy, M. J., McKiernan, E., O'Donovan, N. & McGowan, P. M. Role of ADAMs in cancer formation and progression. *Clin. Cancer Res.* **15**, 1140–1144 (2009).
35. Zelenay, S. et al. Cyclooxygenase-dependent tumor growth through evasion of immunity. *Cell* **162**, 1257–1270 (2015).
36. Eberlein, J. et al. Chemokine signatures of pathogen-specific T cells I: effector T cells. *J. Immunol.* **205**, 2169–2187 (2020).
37. Ng, S. S. et al. The NK cell granule protein NKG7 regulates cytotoxic granule exocytosis and inflammation. *Nat. Immunol.* **21**, 1205–1218 (2020).
38. Aggarwal, V., Workman, C. J. & Vignali, D. A. A. LAG-3 as the third checkpoint inhibitor. *Nat. Immunol.* **24**, 1415–1422 (2023).
39. Santos, R. F. The dual character of the inhibitory functions of CD6. Preprint at *bioRxiv* https://doi.org/10.1101/2022.04.29.490054 (2022).
40. Oliveira, M. I. et al. CD6 attenuates early and late signaling events, setting thresholds for T-cell activation. *Eur. J. Immunol.* **42**, 195–205 (2012).
41. Mori, D. et al. The T cell CD6 receptor operates a multitask signalosome with opposite functions in T cell activation. *J. Exp. Med.* **218**, e20201011 (2021).
42. Castro, M. A. et al. Extracellular isoforms of CD6 generated by alternative splicing regulate targeting of CD6 to the immunological synapse. *J. Immunol.* **178**, 4351–4361 (2007).
43. Te Riet, J. et al. Dynamic coupling of ALCAM to the actin cortex strengthens cell adhesion to CD6. *J. Cell Sci.* **127**, 1595–1606 (2014).
44. Zvezdova, E. et al. Themis1 enhances T cell receptor signaling during thymocyte development by promoting Vav1 activity and Grb2 stability. *Sci. Signal.* **9**, ra51 (2016).
45. Choi, S. et al. THEMIS increases TCR signaling in CD4$^+$CD8$^+$ thymocytes by inhibiting the activity of the tyrosine phosphatase SHP1. *Sci. Signal.* **16**, eade1274 (2023).
46. Fu, G. et al. Themis sets the signal threshold for positive and negative selection in T-cell development. *Nature* **504**, 441–445 (2013).
47. Liu, Y. et al. Themis is indispensable for IL-2 and IL-15 signaling in T cells. *Sci. Signal.* **15**, eabi9983 (2022).

48. Yang, C. et al. THEMIS enhances the magnitude of normal and neuroinflammatory type 1 immune responses by promoting TCR-independent signals. *Sci. Signal.* **15**, eabl5343 (2022).
49. Vigario, A. M. & Pamplona, A. γδ T cells as immunotherapy for malaria: balancing challenges and opportunities. *Front. Immunol.* **14**, 1242306 (2023).

https://doi.org/10.1038/s41590-024-02073-8

Methods

Mice

C57BL/6J mice were purchased from Charles Rivers Laboratories. Double *Il17a*-GFP:*Ifng*-YFP reporter mice were generated and bred in-house by crossing the following single-reporter strains: Great (*Ifng*-YFP)[50], obtained from The Jackson Laboratory, and *Il17*-GFP[51], obtained from Biocytogen. *Cd6*$^{\Delta d3/\Delta d3}$ and *Themis*$^{-/-}$ mouse strains were established in the laboratories of A.M.C.[39] and R.L.[19], respectively. All strains were kept on a C57BL/6J background. All mice were adults (6–14 weeks). Mice were bred and housed on a 14-h light/10-h dark cycle maintained at a temperature of 22–24 °C and relative humidity of 45–65%. All mice were housed in specific opportunistic pathogen-free animal holding rooms, and experiments were performed in specific pathogen-free animal rooms located at the Gulbenkian Institute for Molecular Medicine (GIMM) Rodent Facility. This facility complies with Portuguese law Decreto-Lei 113/2013, transposed from the European Directive 2010/63/EU, and follows the European Commission recommendations (2007/526/EC) on housing and care of animals and the Federation of European Laboratory Animal Science Associations guidelines concerning laboratory animal welfare. All experiments involving mice were approved by the Animal Welfare Body (ORBEA-GIMM), were set up in accordance with Article 34 of Decreto-Lei 113/2013 and were submitted to Direcção-Geral de Alimentação e Veterinária for authorization. Euthanasia was performed by CO_2 inhalation, and anesthesia was performed by isofluorane inhalation.

P. berghei ANKA infection

GFP-expressing *P. berghei* ANKA sporozoites[52] were obtained by dissection of the salivary glands of infected *Anopheles stephensi* mosquitoes bred at the GIMM insectarium. Mice were injected via the retro-orbital route with 100 µl of DMEM containing 2×10^4 sporozoites obtained from the salivary glands of freshly dissected mosquitoes. Parasitemia was measured daily from day 3 onward by analyzing the frequency of GFP$^+$ infected red blood cells through flow cytometry. Simultaneously, mice were monitored daily for signs of ECM, including hemi- or paraplegia, head deviation, a tendency to roll over on stimulation, ataxia and the inability to self-right[3].

EAE induction

Il17a-GFP:*Ifng*-YFP reporter mice were immunized subcutaneously in both flanks with 100 µg of myelin oligodendrocyte glycoprotein 35–55 peptide (MEVGWYRSPFSRVVHLYRNGK; Eurogentec) emulsified in complete Freund's adjuvant solution (4 mg ml^{-1} heat-inactivated *Mycobacterium tuberculosis* in incomplete Freund's adjuvant; Difco Laboratories). On the day of immunization and 2 days after, mice received 200 ng of pertussis toxin (List Biological Laboratories) in 100 µl of PBS via retro-orbital route. Mice were weighed daily and scored for EAE clinical signs. In brief, the score system ranged from 0 to 5, with 0.5 increments, where a score of 0 was assigned to animals with no clinical signs of EAE, a score of 1 was assigned to animals with a limp tail, a score of 2 was assigned to animals with a limp tail and hind leg weakness, a score of 3 was assigned to animals with complete limb paralysis, a score of 4 was assigned to animals with complete hind leg paralysis and partial front paralysis, and a score of 5 was assigned to animals that died.

Tissue processing and cell isolation

For organ collection from *P. berghei*-infected mice, mice were killed at day 5 after infection, and, following transcardiac perfusion with ice-cold PBS, pLNs (cervical, axillary, brachial, inguinal and popliteal) were collected. For organ collection from EAE mice, mice were killed at day 15 after immunization, and, following transcardiac perfusion with ice-cold PBS, LNs (cervical, axillary, brachial, inguinal and lumbar) were collected. Liver and testes were collected following transcardiac perfusion with ice-cold PBS. Single-cell suspensions from (p)LNs, spleens, thymi and livers were prepared by manual straining through a 70/120-µm cell strainer. Single-cell suspensions from testes were prepared by cutting the samples into pieces, followed by a 30-min incubation at 37 °C with shaking in RPMI-1640 medium with L-glutamine supplemented with 5% heat-inactivated fetal calf serum (HI-FCS) containing collagenase D (1.5 mg ml^{-1}; Roche) and DNase I (20 µg ml^{-1}; Roche). Digested samples were then manually strained through a 120-µm cell strainer. Leukocytes from both testis and liver single-cell suspensions were then isolated through a two-step 40%/80% density Percoll gradient centrifuged at 700*g* for 10 min at room temperature with no acceleration or brake. Erythrocytes from spleen, thymus and liver single-cell suspensions were osmotically lysed in red blood cell lysis buffer (BioLegend), followed by washing in ice-cold PBS.

Cell culture

Cells were cultured in complete RPMI, consisting of RPMI-1640 medium with L-glutamine supplemented with 10% HI-FCS, 1% penicillin and streptomycin, 1% HEPES, 1% non-essential amino acids, 0.1% gentamycin and 50 µM β-mercaptoethanol (all reagents from Gibco). For γδ T cell in vitro culture, pLN- and spleen-derived lymphocytes were enriched by magnetic-activated cell sorting by negative selection in LS columns using biotin-conjugated anti-CD11b (M1/70), anti-CD11c (N418), anti-CD19 (6D5), anti-TER-119 (TER-119) and anti-TCRβ (H57-597; Biolegend) and anti-biotin microbeads (Miltenyi Biotec), following the manufacturer's instructions. Enriched samples were stained for cell surface markers and sorted by FACS. Following cell sorting, *Ifng*-YFP:*Il17a*-GFP γδ^{DN}, γδ^{GFP} or γδ^{YFP} cells were stimulated for 16 h with IL-12 (5 ng ml^{-1}; PeproTech) plus IL-18 (5 ng ml^{-1}; PeproTech) or IL-1β (10 ng ml^{-1}; PeproTech) plus IL-23 (10 ng ml^{-1}; R&D Systems) in the presence or absence of plate-bound anti-CD3ε (145-2C11, BioLegend) at 2.50 µg ml^{-1}; *Cd6*$^{WT/WT}$ and *Cd6*$^{\Delta d3/\Delta d3}$ CD27$^{-/+}$ γδ cells were labeled with CTV (Invitrogen) following the manufacturer's instructions. These cells were then cocultured in the presence or absence of soluble anti-CD3ε at 0.25, 0.625, 1.25 or 2.50 µg ml^{-1} for 48–72 h at 37 °C and 5% CO_2 at a 1:10 ratio with T cell-depleted splenocytes stained with CellTrace CFSE (Invitrogen). *Themis*$^{+/-}$ and *Themis*$^{-/-}$ γδ T cells were labeled with CTV and stimulated with plate-bound anti-CD3ε plus anti-CD28 (37.51, Invitrogen) at 0.25, 0.625, 1.25 and 2.50 µg ml^{-1} for 48–72 h.

Fluorochrome-conjugated monoclonal antibodies

The following anti-mouse fluorochrome-conjugated monoclonal antibodies to cell surface or intracellular molecules were used (with identification of clones and dilutions): CD3ε (17A2 or 145-2C11, 1:200), CD6 (OX-129, 1:200), CD24 (M1/69, 1:400), CD25 (PC61 or 3C7, 1:200), CD27 (LG.3A10 or LG.7F9, 1:200), CD44 (IM7, 1:400), CD45 (30-F11, 1:400), CD45RB (C363.16A, 1:200), CD69 (H1.2F3, 1:200), CD122 (TM-β1, 1:200), IFNγ (XMG1.2, 1:100), IL-17A (TC11-18H10, 1:100), Ki-67 (16A8, 1:200), TCRδ (GL3, 1:200), Themis (1TMYS, 1:100), Vγ1 (2.11, 1:200), Vγ4 (UC3-10A6, 1:200) and Vγ5 (536, 1:200). Antibodies were purchased from BD Biosciences, BioLegend, eBioscience or Invitrogen.

Flow cytometry and cell sorting

For cell sorting of γδ T cell subsets from the *Il17a*-GFP:*Ifng*-YFP reporter mouse model, cells were stimulated for 3 h at 37 °C in complete RPMI containing 50 ng ml^{-1} PMA and 1 µg ml^{-1} ionomycin (both from Sigma). For cell surface staining, thymocytes and lymphocytes were resuspended in FACS buffer (PBS with 2% HI-FCS) containing fluorochrome-conjugated antibodies and LIVE/DEAD Fixable Near IR (780) Viability Dye (Invitrogen) in the presence of anti-CD16/CD32 (eBiosciences) and incubated for 15 min at 4 °C in the dark. After staining, cells were washed and resuspended in FACS buffer for flow cytometry cell analysis or complete RPMI for cell sorting. For intracellular detection of IL-17A, IFNγ and Ki-67, cells were first stimulated with 25 ng ml^{-1} PMA and 1 µg ml^{-1} ionomycin for 3 h at 37 °C in the presence of 1 µg ml^{-1} Brefeldin A (Sigma). After cell surface staining was

performed as described earlier, cells were fixed and permeabilized with the Foxp3/Transcription Factor buffer set (eBioscience) following the manufacturer's instructions and subsequently stained with fluorochrome-conjugated antibodies in the presence of anti-CD16/CD32 for 30 min at 4 °C in the dark. For intracellular cytokine staining of GFP$^+$/YFP$^+$ samples, cells were fixed in 2% paraformaldehyde and permeabilized with Permeabilization Buffer (eBioscience) in the presence of anti-CD16/CD32 for 15 min, after which intracellular staining was performed by adding antibodies to cytokines in the indicated permeabilization buffer and incubating for 30 min at 4 °C in the dark. For intracellular detection of Themis, after cell surface staining, samples were fixed in 2% paraformaldehyde, permeabilized and stained with PBS containing 0.5% Triton X-100, and washed three times with PBS. All samples were acquired in FACS buffer using one of the following cell analyzers: BD LSRFortessa, BD LSRFortessa X20 (FACSDiva software, BD Biosciences) or Cytek Aurora (SpectroFlo software, Cytek). Data were analyzed using FlowJo software (FlowJo). Cell sorting was performed with a 70-µm nozzle on a BD FACSAria II, III or Fusion (FACSDiva software, BD Biosciences). Sorted cells were washed in PBS and used for culture or frozen in liquid nitrogen and kept at −80 °C for RNA extraction.

RNA isolation, cDNA synthesis and RT–qPCR

RNA was isolated from cell populations sorted by FACS using an miRNeasy Mini kit (Qiagen). Reverse transcription was performed with random oligonucleotides (Invitrogen) using Moloney murine leukemia virus reverse transcriptase (Promega). Relative quantification of specific cDNA species to the endogenous reference *Actb* or *B2m* was performed using SYBR on a ViiA7 cycler (Applied Biosystems). Primers were either designed manually or by the Universal ProbeLibrary Assay Design Center (Roche), and their sequences are indicated in Supplementary Table 8. Relative quantification was performed using the change in cycling threshold ($\Delta\Delta C_t$) method.

RNA-seq

Deep sequencing (RNA-seq) was performed at the GeneCore facility of EMBL (http://www.genecore.embl.de/). Libraries were prepared according to the Illumina protocol and were subjected to paired-end sequencing on a HiSeq2000 system.

RNA-seq data analysis

Sequenced reads were aligned to the mouse genome (GRCm38) using Hisat2 (ref. 53), and gene count tables were obtained using featureCounts[54] against mouse gene models (gencode M16). Low-expressed genes were filtered out using the edgeR R package[55]. Library sizes were normalized using the trimmed mean of M values (TMM) method in edgeR[56]. Differential expression analysis between groups was performed using an empirical Bayes quasilikelihood approach in edgeR[57]. Genes were considered differentially expressed if the FDR of the quasilikelihood test was less than 0.05 and the estimated fold change between groups was greater than 1.5. For display purposes, counts were transformed to normalized $\log_2$ (CPM) values. GO enrichment analysis of hierarchical clusters was performed using GOrilla[58].

Computational analysis of single-cell RNA-seq data

Single-cell data from Yang et al.[14] and du Halgouet et al.[15] were processed using Seurat[59]. Barcode–gene matrices from Yang et al. were downloaded from https://www.ncbi.nlm.nih.gov/geo/query/acc.cgi?acc=GSM6927021 and processed with Seurat to remove low-quality cells (genes > 200, features of >1,000 and <3,000, percentage of mitochondrial genes of <5). Cells with *Il17a* or *Ifng* counts were then subsetted, counts were normalized and scaled, and differential expression analysis was performed between *Il17a*$^+$ and *Ifng*$^+$ cells using the FindMarkers function. For du Halgouet et al., processed Seurat data were obtained from https://github.com/sagar161286/multimodal_gdT-cells. The Seurat object was subsetted to include only cells with either *Il17a* or *Ifng* read counts (a very small number of double-positive cells were excluded), and a similar analysis to the one described earlier was performed.

Statistical analysis

No statistical methods were used to predetermine sample sizes, but our sample sizes are similar to those reported in previous publications[9,10,25]. Statistical analyses were performed using GraphPad Prism. Where parametric tests were used, data distribution was either tested using a Kolmogorov–Smirnov test or was assumed to be normal according to the information provided in the respective figure captions. Outliers in RT–qPCR data were detected and excluded through a Grubbs's test, also known as the extreme studentized deviate method.

Reporting summary

Further information on research design is available in the Nature Portfolio Reporting Summary linked to this article.

Data availability

γδ T cell RNA-seq data have been deposited in the Sequence Read Archive repository in NCBI under accession code PRJNA1080348, and CD4$^+$ T cell RNA-seq data are also available from the Sequence Read Archive under accession code PRJNA1067547. All other data that support the findings of this study are available in the article and Supplementary Information or from the corresponding authors upon request.

References

50. Reinhardt, R. L., Liang, H. E. & Locksley, R. M. Cytokine-secreting follicular T cells shape the antibody repertoire. *Nat. Immunol.* **10**, 385–393 (2009).
51. Lee, Y. et al. Induction and molecular signature of pathogenic T_H17 cells. *Nat. Immunol.* **13**, 991–999 (2012).
52. Franke-Fayard, B. et al. A *Plasmodium berghei* reference line that constitutively expresses GFP at a high level throughout the complete life cycle. *Mol. Biochem. Parasitol.* **137**, 23–33 (2004).
53. Kim, D., Paggi, J. M., Park, C., Bennett, C. & Salzberg, S. L. Graph-based genome alignment and genotyping with HISAT2 and HISAT-genotype. *Nat. Biotechnol.* **37**, 907–915 (2019).
54. Liao, Y., Smyth, G. K. & Shi, W. featureCounts: an efficient general purpose program for assigning sequence reads to genomic features. *Bioinformatics* **30**, 923–930 (2014).
55. Robinson, M. D., McCarthy, D. J. & Smyth, G. K. edgeR: a Bioconductor package for differential expression analysis of digital gene expression data. *Bioinformatics* **26**, 139–140 (2010).
56. Robinson, M. D. & Oshlack, A. A scaling normalization method for differential expression analysis of RNA-seq data. *Genome Biol.* **11**, R25 (2010).
57. Robinson, M. D. & Smyth, G. K. Moderated statistical tests for assessing differences in tag abundance. *Bioinformatics* **23**, 2881–2887 (2007).
58. Eden, E., Navon, R., Steinfeld, I., Lipson, D. & Yakhini, Z. GOrilla: a tool for discovery and visualization of enriched GO terms in ranked gene lists. *BMC Bioinform.* **10**, 48 (2009).
59. Hao, Y. et al. Integrated analysis of multimodal single-cell data. *Cell* **184**, 3573–3587 (2021).

Acknowledgements

We thank our colleagues, N. Gonçalves-Sousa, J. Ribot, K. Serre, G. Fiala, J. Darrigues, V. Zuzarte-Luís and A. Parreira as well as F. Enguita and M. Costa for help and discussions on RNA-seq data analysis and deposition, H. Pinheiro for support in the design of the schematics (Gulbenkian Institute for Molecular Medicine, Lisbon), D. Pennington (Queen Mary University of London) for insightful discussions and/or technical advice and the staff of the rodent and flow cytometry facilities of our institutes for their critical support. We thank V. Benes

and his team at the European Molecular Laboratory GeneCore facility for assistance with library preparation for the RNA-seq analyses. The project leading to these results has received funding from the European Research Council under the European Union's Horizon 2020 research and innovation programme (grant agreement number 646701 to B.S.-S.), 'la Caixa' Foundation under project code LCF/PR/HR24/00929 (to B.S.-S.), Fundação para a Ciência e Tecnologia, Ministério da Ciência, Tecnologia e Ensino Superior, Portugal (PTDC/MED-IMU/32296/2017 to A.M.C.; SFRH/BD/145352/2019 to D.I.; Decree-law number 57/2016, as amended by the Law number 57/2017 to A.P.) and Fondation pour la Recherche Médicale (to R.L.).

Author contributions

D.I. (Figs. 4–7, including validation of the gene panel and functional analyses), T.A. (Figs. 1–3, including establishment of the reporter mouse model, RNA-seq and enrichment/pathway analyses) and A.P. (Figs. 4, 6 and 7, including validation of the gene panel and functional analyses) performed most of the experiments and analyzed the data. D.S., C.C., R.F.S., L.O. and N.R. provided technical assistance in some experiments. A.M.C. and R.L. provided materials and support. A.Q.G. and B.S.-S. conceived and supervised the research and wrote the paper.

Competing interests

The authors declare no competing interests.

Additional information

Extended data is available for this paper at https://doi.org/10.1038/s41590-024-02073-8.

Supplementary information The online version contains supplementary material available at https://doi.org/10.1038/s41590-024-02073-8.

Correspondence and requests for materials should be addressed to Anita Q. Gomes or Bruno Silva-Santos.

Peer review information *Nature Immunology* thanks Ben Willcox and the other, anonymous, reviewer(s) for their contribution to the peer review of this work. Primary Handling Editor: Nick Bernard, in collaboration with the *Nature Immunology* team.

https://doi.org/10.1038/s41590-024-02073-8

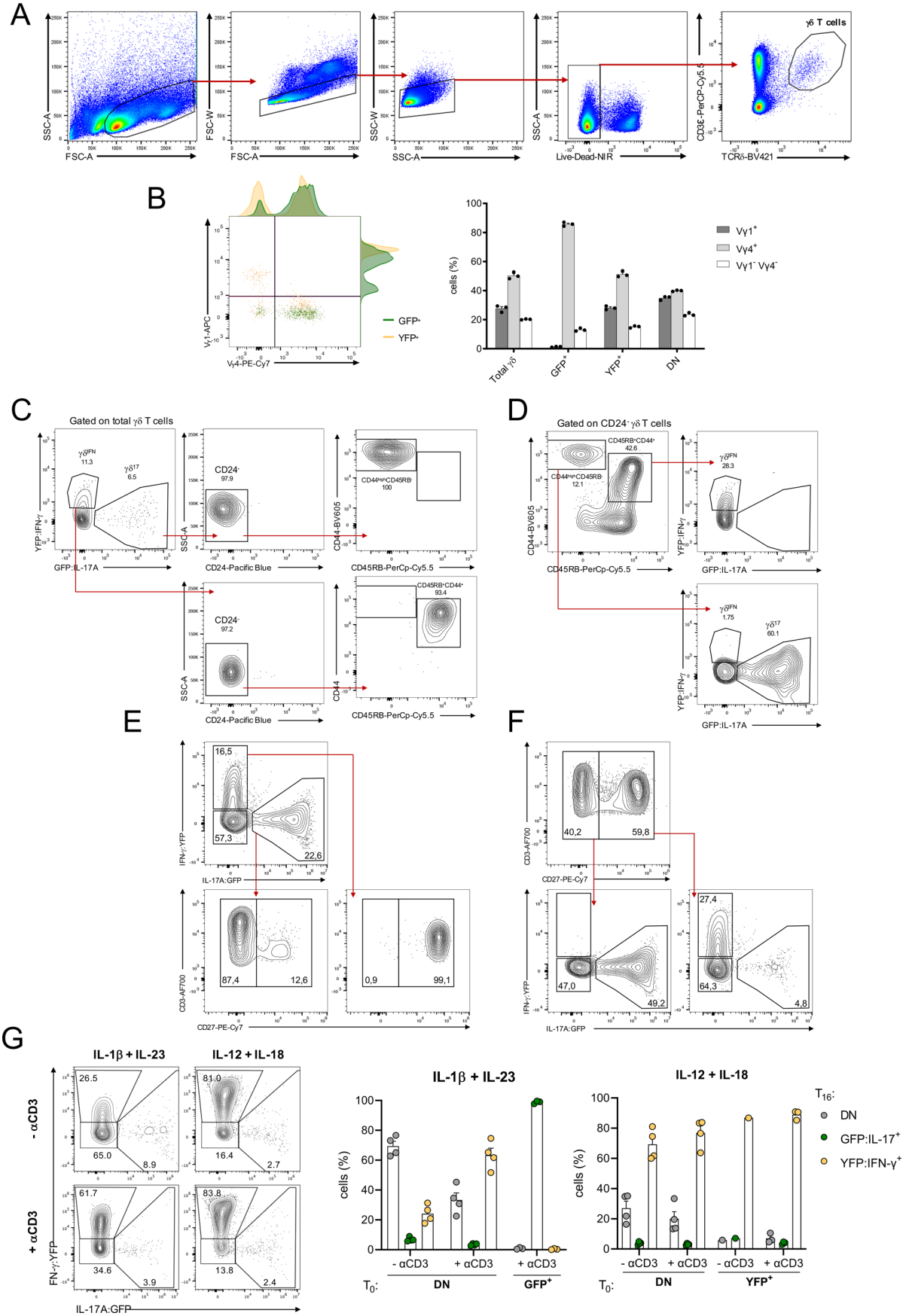

Extended Data Fig. 1 | See next page for caption.

https://doi.org/10.1038/s41590-024-02073-8

Extended Data Fig. 1 | Characterization of γδ T cell subsets isolated from Il17a-GFP:Ifng-YFP reporter mice. (a) Representative flow cytometry plots showing gating strategy used to identify γδ T cells subsets. Red arrows show sequence of gating strategy. **(b)** Characterization of the V_γ chain usage, as determined by $V_\gamma1$ and $V_\gamma4$ TCR staining, within the GFP$^+$, YFP$^+$ and DN γδ T cell populations of *Il17a*-GFP:*Ifng*-YFP reporter mice (n = 3 mice). Data are representative of one independent experiment and each symbol represents a biological replicate. **(c)** Representative flow cytometry plots displaying the expression of CD24, CD44 and CD45RB extracellular markers within the GFP$^+$, YFP$^+$ and DN γδ T cell subsets from the pLN of *Il17a*-GFP:*Ifng*-YFP reporter mice, and **(d)** the expression of GFP and YFP within CD24$^-$ CD44^{high}CD45RB$^-$ or CD45RB$^+$CD44$^+$ γδ T cell subsets from the pLN of reporter mice. **(e)** Representative flow cytometry plots displaying the expression of CD27 within the GFP$^+$, YFP$^+$ and DN γδ T cell subsets from the pLN of *Il17a*-GFP:*Ifng*-YFP reporter mice and **(f)** the expression of GFP and YFP within CD27$^-$ or CD27$^+$ γδ T cell subsets from the pLN of reporter mice. **(g)** Representative flow cytometry plots and barplots displaying the frequencies of $γδ^{DN}$, $γδ^{17}$ (GFP$^+$) or $γδ^{IFN}$ (YFP$^+$) cells after 16 h of *in vitro* differentiation of $γδ^{DN}$ sorted from the pooled pLN plus spleen of *Il17a*-GFP:*Ifng*-YFP reporter mice, cultured wither with IL-1β plus IL-23 or IL-12 plus IL-18 in the presence or absence of p.b. anti-CD3 mAb. Data are representative of two independent experiments and each symbol represents a biological replicate. Graphs display Mean ± SEM.

https://doi.org/10.1038/s41590-024-02073-8

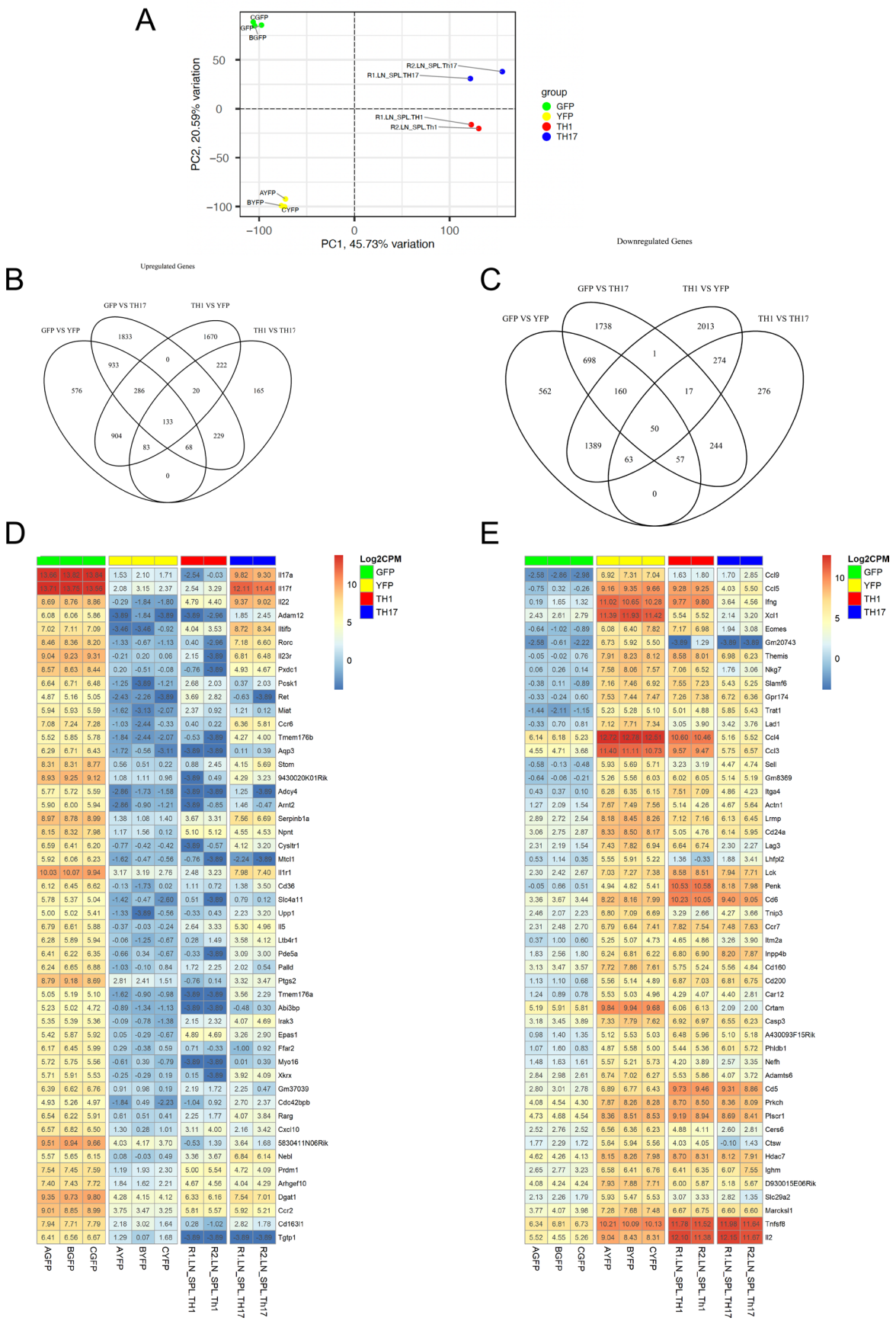

Extended Data Fig. 2 | See next page for caption.

https://doi.org/10.1038/s41590-024-02073-8

Extended Data Fig. 2 | Comparison of expression profiles of effector γδ and CD4 + T cell subsets. (a) PCA plot from mRNA-seq data analysis, comprising the three GFP and three YFP samples from pLN γδ T cell subsets, and two Th17 and two Th1 samples also isolated from *Il17a*-GFP:*Ifng*-YFP reporter mice but at the peak of experimental autoimmune encephalomyelitis (EAE). Each population of cells isolated – GFP^+ (labelled GFP, in green); YFP^+ (labelled YFP, in yellow), Th1 (in red) and Th17 (in blue) – is represented by its independent samples. **(b)** Venn diagram of the upregulated genes (FDR < 0.05 and fold change > 1.5) of the different comparison pairs. **(c)** Venn diagram of the downregulated genes (FDR < 0.05 and fold change > 1.5) of the different comparison pairs. **(d)** Heatmap displaying the $\log_2$(CPM) normalized expression values of the most enriched (ordered by fold change) differentially expressed genes in $\gamma\delta^{17}$ and comparison with Th1 and Th17 profiles. **(e)** Heatmap displaying the $\log_2$(CPM) normalized expression values of the most enriched (ordered by fold change) differentially expressed genes in $\gamma\delta^{IFN}$ and comparison with Th1 and Th17 profiles.

https://doi.org/10.1038/s41590-024-02073-8

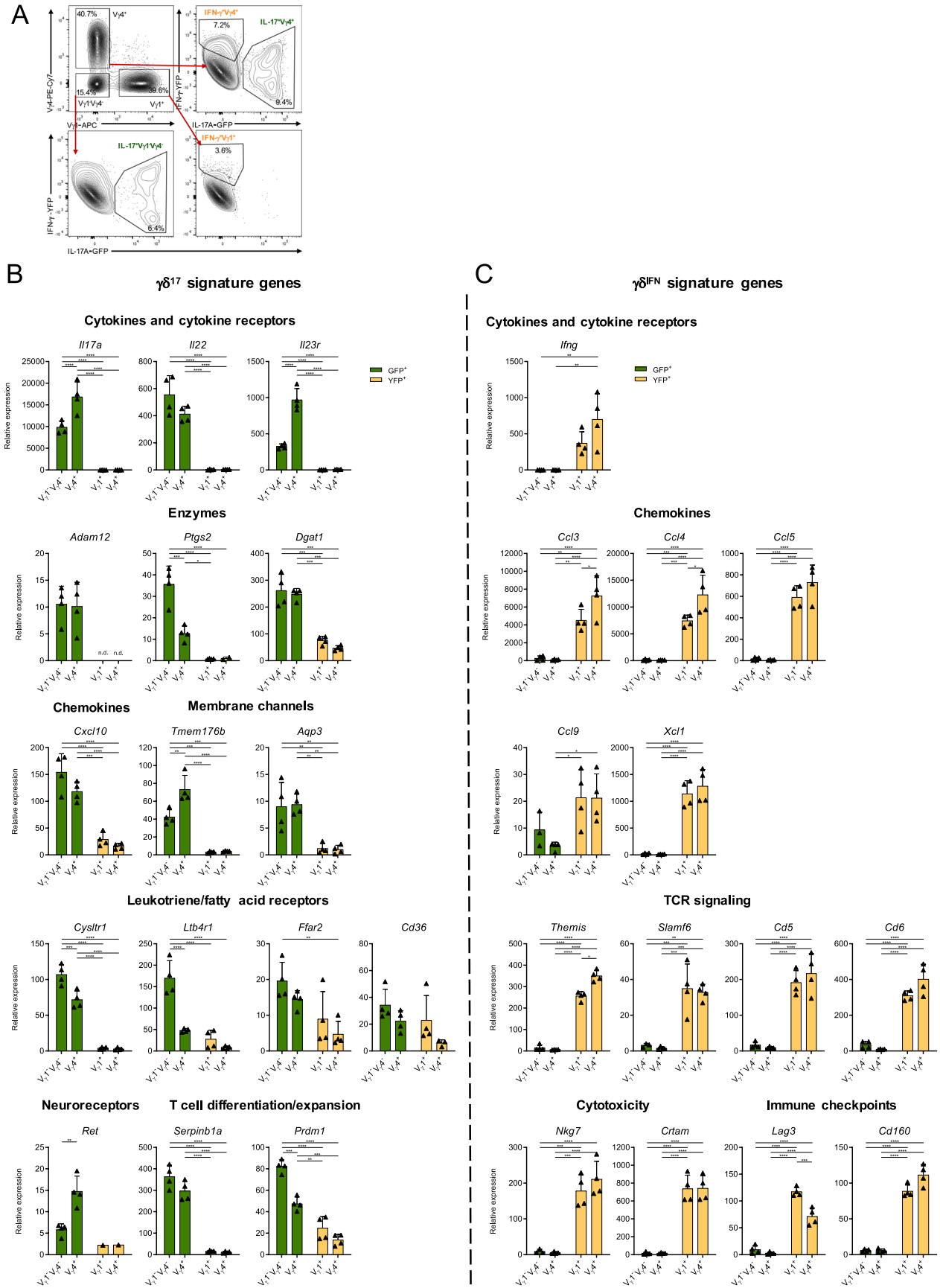

Extended Data Fig. 3 | See next page for caption.

https://doi.org/10.1038/s41590-024-02073-8

Extended Data Fig. 3 | Expression of signature genes in Vγ-based subsets of γδ^{17} or γδ^{IFN} cells. (a) γδ^{17} GFP^{+}V$_{\gamma}$1^{-}V$_{\gamma}$4^{-} and GFP^{+}V$_{\gamma}$4^{+} and γδ^{IFN} YFP^{+}V$_{\gamma}$1^{+} and YFP^{+}V$_{\gamma}$4^{+} cells were sorted and RNA was extracted and subject to RT-qPCR analysis. Relative expression levels of **(b)** γδ^{17} signature genes or **(c)** γδ^{IFN} signature genes were normalised to β-actin (n = 4). Data are representative of one to four independent experiments. Each symbol is a pool of cells from several mice. Graphs display Mean ± SEM. One-way analysis of variance (ANOVA) test with Tukey's multiple-comparisons test under the assumption of data normality. P* ≤ 0.05, **P ≤ 0.01, ***P ≤ 0.001, ****P ≤ 0.0001.

https://doi.org/10.1038/s41590-024-02073-8

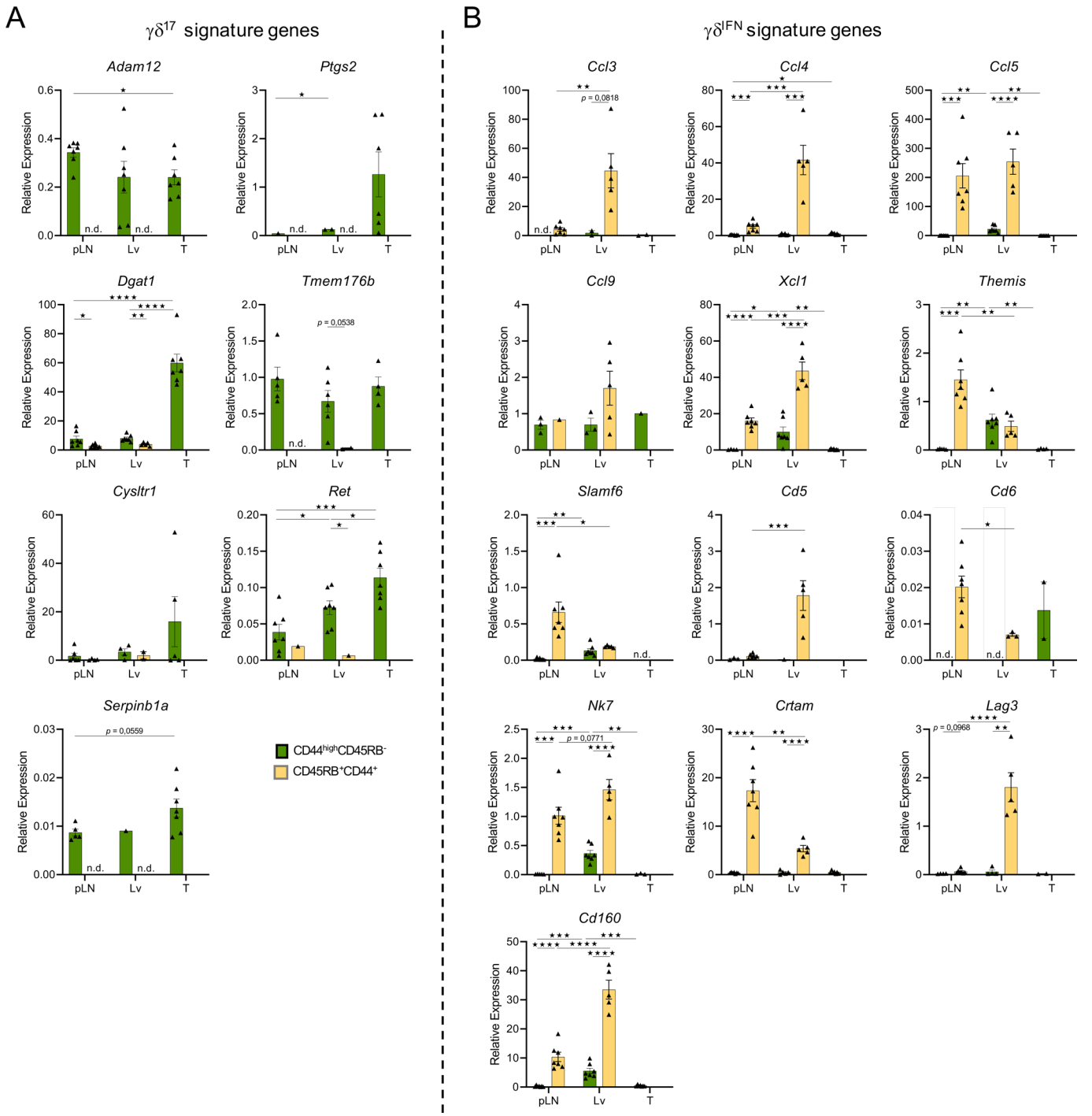

Extended Data Fig. 4 | Expression of γδ^{17}/γδ^{IFN} signature genes in *ex vivo* γδ^{17}-biased CD44^{high}CD45RB^{-} or γδ^{IFN}-biased CD45RB^{+}CD44^{+} cells. **(a-b)** Relative expression levels of (A) γδ^{17} and (B) γδ^{IFN} signature genes normalized to *B2m* (β2-microglobulin) in *ex vivo* CD24^{-}CD44^{high}CD45RB^{-} and CD24^{-}CD45RB^{+}CD44^{+} γδ T cells sorted from the pLN, liver (Lv) or testis (T) of C57BL/6 mice; n.d. means non-detected. Data are representative of seven independent experiments. Each symbol is a pool of cells from several mice. Graphs display Mean ± SEM. Two-tailed *t*-tests were performed under the assumption of data normality. P* ≤ 0.05, **P ≤ 0.01, ***P ≤ 0.001, ****P ≤ 0.0001.

https://doi.org/10.1038/s41590-024-02073-8

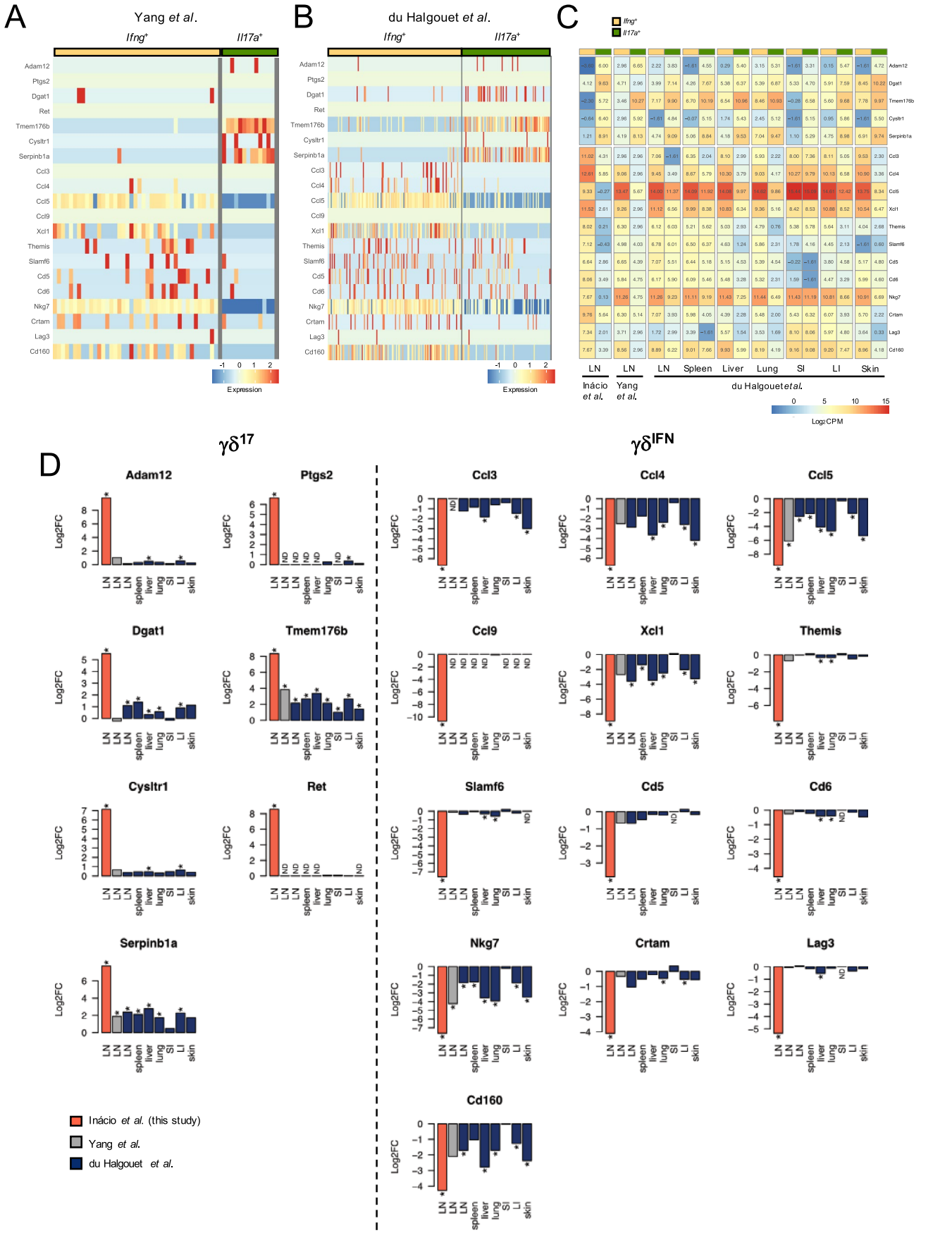

Extended Data Fig. 5 | See next page for caption.

https://doi.org/10.1038/s41590-024-02073-8

Extended Data Fig. 5 | Comparison of the expression of the γδ^{17}/γδ^{IFN} signature genes in our bulk RNA-seq with publicly available scRNA-seq datasets. (a-b) Heatmaps depicting the normalized scaled Seurat expression values for each of the 20 validated γδ^{17}/γδ^{IFN} signature genes identified in our study in *Il17a*+ or *Ifng* + γδ T cells from the publicly-available Yang *et al*.[16] (A) or du Halgouet *et al*.[17] (B) single-cell RNA-seq datasets. **(c)** Heatmap displaying the $\log_2$(CPM) normalized expression values from pseudobulk counts of the 20 validated γδ^{17}/γδ^{IFN} signature genes in *Il17a*+ or *Ifng* + γδ T cells from our dataset (LN) or those of of Yang *et al*. (LN) and du Halgouet *et al*. [LN, spleen, liver, lung, small intestine (SI), large intestine (LI) and skin] and **(d)** barplots displaying $\log_2$(FC) estimated values of the validated γδ^{17}/γδ^{IFN} signature genes between those same *Il17a*+ or *Ifng* + γδ T cells from the three datasets.

https://doi.org/10.1038/s41590-024-02073-8

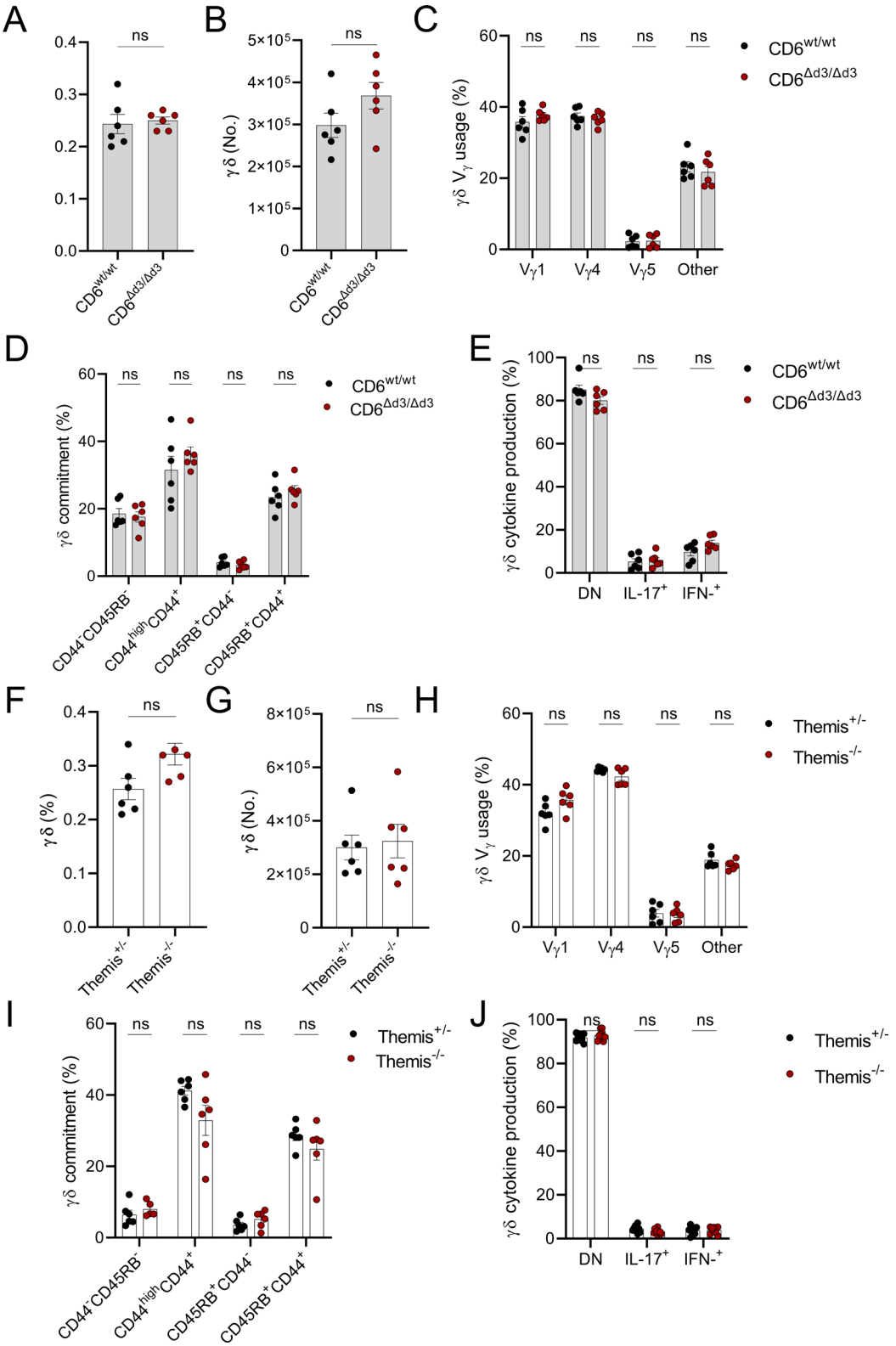

Extended Data Fig. 6 | See next page for caption.

https://doi.org/10.1038/s41590-024-02073-8

Extended Data Fig. 6 | Analysis of thymic γδ T cell subsets in CD6 mutant or Themis-deficient mice. **(a)** Frequency and **(b)** total cell counts of γδ T cells in the thymus of adult $CD6^{\Delta d3/\Delta d3}$ and littermate CD6 control mice. **(c)** Frequency of V_γ usage of γδ T cells in the thymus of adult $CD6^{\Delta d3/\Delta d3}$ and littermate CD6 control mice. **(d)** Frequency of thymic γδ T cells committed to the $CD24^-$ $CD44^-CD45RB^-$, $CD44^{high}CD45RB^-$, $CD45RB^+CD44^-$ and $CD45RB^+CD44^+$ subsets in the thymus of adult $CD6^{\Delta d3/\Delta d3}$ and littermate CD6 control mice. **(e)** Frequency of IL-17^+, IFN-γ^+ or IL-17^-IFN-γ^- double negative (DN) γδ T cells from the thymus of adult $CD6^{\Delta d3/\Delta d3}$ and littermate CD6 control mice upon *in vitro* stimulation with PMA/ionomycin in the presence of Brefeldin A. **(f)** Frequency and **(g)** total cell counts of γδ T cells in the thymus of adult $Themis^{-/-}$ and littermate $Themis^{+/-}$ control mice. **(h)** Frequency of Vγ usage of γδ T cells in the thymus of adult $Themis^{-/-}$ and littermate $Themis^{+/-}$ control mice. **(i)** Frequency of thymic γδ T cells committed to the $CD24^-$ $CD44^-CD45RB^-$, $CD44^{high}CD45RB^-$, $CD45RB^+CD44^-$ and $CD45RB^+CD44^+$ subsets in the thymus of adult $Themis^{-/-}$ and littermate $Themis^{+/-}$ control mice. **(j)** Frequency of IL-17^+, IFN-γ^+ or IL-17^-IFN-γ^- double negative (DN) γδ T cells from the thymus of adult $Themis^{-/-}$ and littermate $Themis^{+/-}$ control mice upon *in vitro* stimulation with PMA/ionomycin in the presence of Brefeldin A. All data are representative of two independent experiments ($n = 6$ mice), and each symbol represents a biological replicate. Graphs display Mean ± SEM. Two-tailed Mann-Whitney (A-B, F-G) or multiple comparisons Kruskal-Wallis (C-E, H-J) tests.

https://doi.org/10.1038/s41590-024-02073-8

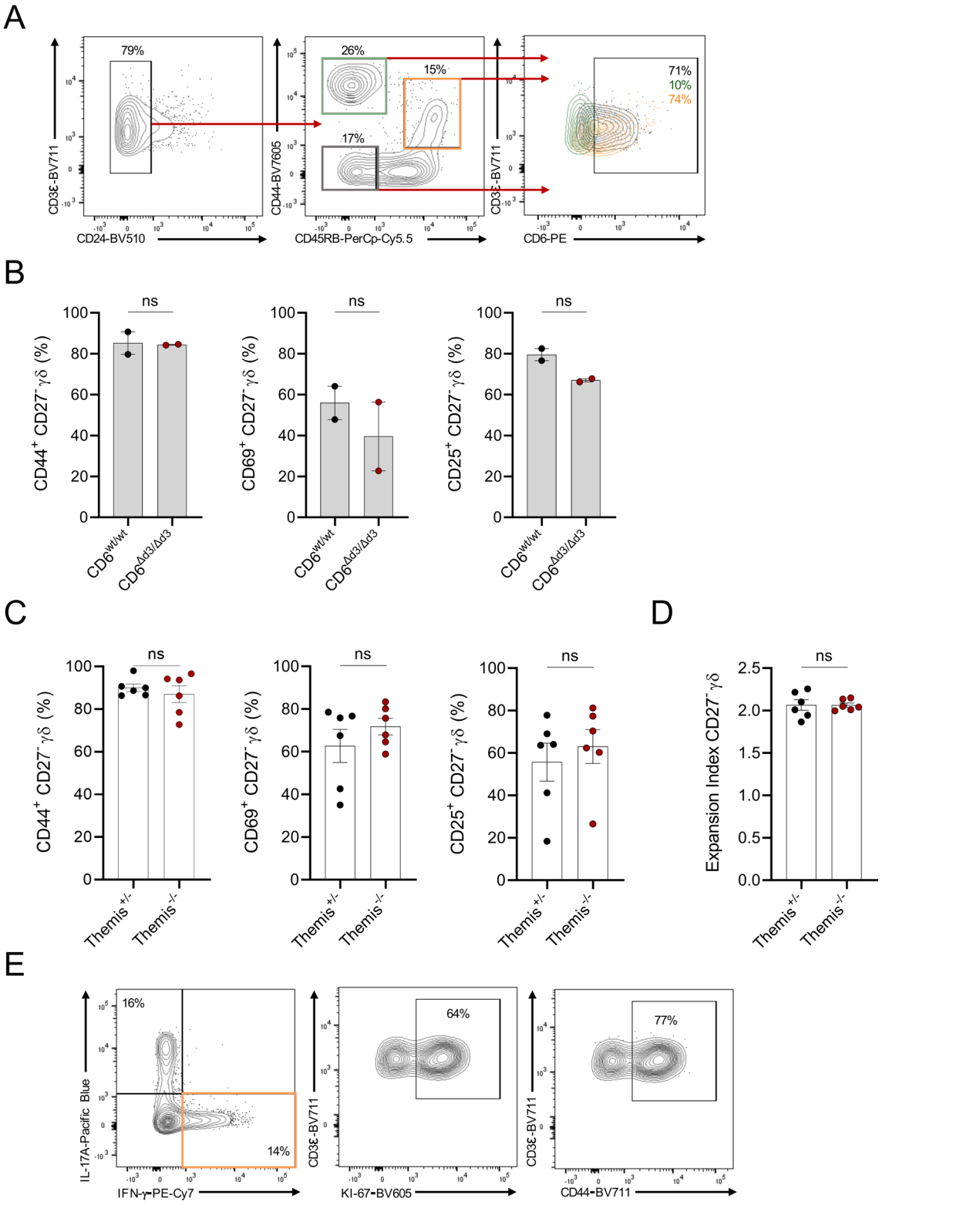

Extended Data Fig. 7 | Activation and proliferation of peripheral γδ^{17}-biased CD27$^-$ γδ T cells from CD6 mutant or Themis-deficient mice. (**a**) Gating strategy used to identify the CD24$^-$ γδ T cell subsets in which CD6 or Themis protein expression was analysed: CD44$^-$CD45RB$^-$, CD44^{high}CD45RB$^-$ and CD45RB$^+$CD44$^+$, with a representative plot of CD6 expression in the three subsets. (**b**) Frequencies of CD44, CD69 and CD25 expression in CTV-labelled CD27$^-$ γδ T cells sorted from pooled pLN and spleen of CD6$^{\Delta d3/\Delta d3}$ or littermate CD6 control mice stimulated for 48 hours with soluble anti-CD3 (1.25 µg/mL) in the presence of T cell-depleted splenocytes. Data are from two independent experiments, n = 2. Each symbol represents a pool of cells from three mice (**c**) Frequencies of CD44, CD69 and CD25 expression and (**d**) expansion index of CTV-labelled CD27$^-$ γδ T cells sorted from pooled pLN and spleen of Themis$^{-/-}$ and littermate Themis$^{+/-}$ control mice upon 48 hours of *in vitro* stimulation with plate-bound anti-CD3 and anti-CD28 (2.5 µg/mL). Themis data are representative of six independent experiments, n = 6; each symbol in the graphs represents a pool of cells from two mice used in each experiment. (**e**) Gating strategy used to identify IFN-γ$^+$ γδ T cells from the pLN of *P. berguei* infected mice at day 5 post infection, with representative plots of KI-67 and CD44 expression in these cells. Graphs display Mean ± SEM. Two-tailed Mann-Whitney test.

nature portfolio

Corresponding author(s): Anita Q. Gomes and Bruno Silva-Santos

Last updated by author(s): Dec 12, 2024

Reporting Summary

Nature Portfolio wishes to improve the reproducibility of the work that we publish. This form provides structure for consistency and transparency in reporting. For further information on Nature Portfolio policies, see our Editorial Policies and the Editorial Policy Checklist.

Statistics

For all statistical analyses, confirm that the following items are present in the figure legend, table legend, main text, or Methods section.

n/a	Confirmed
☐	☒ The exact sample size (*n*) for each experimental group/condition, given as a discrete number and unit of measurement
☐	☒ A statement on whether measurements were taken from distinct samples or whether the same sample was measured repeatedly
☐	☒ The statistical test(s) used AND whether they are one- or two-sided *Only common tests should be described solely by name; describe more complex techniques in the Methods section.*
☒	☐ A description of all covariates tested
☐	☒ A description of any assumptions or corrections, such as tests of normality and adjustment for multiple comparisons
☐	☒ A full description of the statistical parameters including central tendency (e.g. means) or other basic estimates (e.g. regression coefficient) AND variation (e.g. standard deviation) or associated estimates of uncertainty (e.g. confidence intervals)
☐	☒ For null hypothesis testing, the test statistic (e.g. *F*, *t*, *r*) with confidence intervals, effect sizes, degrees of freedom and *P* value noted *Give P values as exact values whenever suitable.*
☒	☐ For Bayesian analysis, information on the choice of priors and Markov chain Monte Carlo settings
☒	☐ For hierarchical and complex designs, identification of the appropriate level for tests and full reporting of outcomes
☒	☐ Estimates of effect sizes (e.g. Cohen's *d*, Pearson's *r*), indicating how they were calculated

Our web collection on statistics for biologists contains articles on many of the points above.

Software and code

Policy information about availability of computer code

Data collection	RNA-sequencing was performed on HiSeq2000 system (Illumina). All flow cytometry data were acquired using FACSDiva 6.2 and FACSDiva 8.0 (BD Biosciences) or SpectroFlo (Cytek). Cell sorting was performed using FACSDiva 6.1.3 or FACSDiva 9.0 software (BD Biosciences). RT-qPCR data were adquired using ViiA 7 1.2.1 sofware (Applied Biosystems).
Data analysis	All analysis are described in the relevant section of Methods. Regarding RNA-seq analysis: sequenced reads were aligned to the mouse genome using Hisat2 (v2.1.0, https://doi.org/10.1038/s41587-019-0201-4), and gene count tables were obtained using featureCounts (v2.0.3, https://doi.org/10.1093/bioinformatics/btt656) against the mouse gene models (gencode M16); low-expressed genes were filtered out using the edgeR R package (v3.32.1, https://doi:10.1093/bioinformatics/btp616); library sizes were normalized using the trimmed mean of M values (TMM) method in edgeR (https://doi.org/10.1186/gb-2010-11-3-r25); and differential expression analysis between groups was performed using an empirical Bayes quasi-likelihood approach in edgeR (https://doi.org/10.1093/bioinformatics/btm453). GO enrichment analysis of hierarchical clusters was performed using GOrilla (https://doi.org/10.1186/1471-2105-10-48). Computational analysis of published single-cell RNA-Seq data sets was done using Seurat (v4). Flow cytometry data were analysed using FlowJo v10.7.2 software (FlowJo LLC). RT-qPCR data was analysed using ViiA 7 1.2.1 sofware (Applied Biosystems). Statistical analysis were done with GraphPad Prism (v8.4.3) software.

For manuscripts utilizing custom algorithms or software that are central to the research but not yet described in published literature, software must be made available to editors and reviewers. We strongly encourage code deposition in a community repository (e.g. GitHub). See the Nature Portfolio guidelines for submitting code & software for further information.

Data

Policy information about availability of data

All manuscripts must include a data availability statement. This statement should provide the following information, where applicable:

- Accession codes, unique identifiers, or web links for publicly available datasets
- A description of any restrictions on data availability
- For clinical datasets or third party data, please ensure that the statement adheres to our policy

gamma-delta T cell RNA-seq data have been deposited in the Sequence Read Archive (SRA) repository in NCBI under the accession code PRJNA1080348 (https://www.ncbi.nlm.nih.gov/bioproject/PRJNA1080348) and CD4+ T cell RNA-seq data are also available from SRA under the accession code PRJNA1067547 (https://www.ncbi.nlm.nih.gov/bioproject/PRJNA1067547). All other data that support the findings of this study are available in the article and Supplementary Information, or from the corresponding authors upon request.

Research involving human participants, their data, or biological material

Policy information about studies with human participants or human data. See also policy information about sex, gender (identity/presentation), and sexual orientation and race, ethnicity and racism.

Reporting on sex and gender	n/a
Reporting on race, ethnicity, or other socially relevant groupings	n/a
Population characteristics	n/a
Recruitment	n/a
Ethics oversight	n/a

Note that full information on the approval of the study protocol must also be provided in the manuscript.

Field-specific reporting

Please select the one below that is the best fit for your research. If you are not sure, read the appropriate sections before making your selection.

☒ Life sciences ☐ Behavioural & social sciences ☐ Ecological, evolutionary & environmental sciences

For a reference copy of the document with all sections, see nature.com/documents/nr-reporting-summary-flat.pdf

Life sciences study design

All studies must disclose on these points even when the disclosure is negative.

Sample size	No sample size calculation was performed; sample size was based on experiences giving reproducible results: experiments whose results presented a bigger signal-to-noise ratio required a higher number of replicates, while experiments whose results presented decreased variability allowed for conclusions with less replicates. Each single experimental was performed multiple times using independent samples.
Data exclusions	Outliers in RT-qPCR data were detected and excluded through Grubbs' test, also known as the ESD method (extreme studentized deviate).
Replication	All data presented in the manuscript derives from independent experiments performed at least twice with samples sourcing from distinct organisms.
Randomization	Mice were assigned randomly to different groups, respecting genotype, age and sex matching, and each given a code number. Samples were treated uniformly, with the same procedure being applied to all simultaneously at a given experiment. Each sample was then assigned its ID after data was analysed.
Blinding	All experiments including knockout or mutant mice and control groups were performed blindly by investigators until analysis of results, including ECM onset evaluation. Other than that, no blinding was involved, given there was no subjective measurements.

Reporting for specific materials, systems and methods

We require information from authors about some types of materials, experimental systems and methods used in many studies. Here, indicate whether each material, system or method listed is relevant to your study. If you are not sure if a list item applies to your research, read the appropriate section before selecting a response.

Materials & experimental systems

n/a	Involved in the study
☐	☒ Antibodies
☒	☐ Eukaryotic cell lines
☒	☐ Palaeontology and archaeology
☐	☒ Animals and other organisms
☒	☐ Clinical data
☒	☐ Dual use research of concern
☒	☐ Plants

Methods

n/a	Involved in the study
☒	☐ ChIP-seq
☐	☒ Flow cytometry
☒	☐ MRI-based neuroimaging

Antibodies

Antibodies used

The following antibodies [Ab (Clone) Fluorochrome, Supplier name, Catalog number] were used for:
1. Flow cytometry:
CD3e (145-2C11) PerCP-Cy5.5, BioLegend, Cat# 100328,
CD3e (17A2) APC-eFluor 780, eBioscience, Cat# 47-0032-82
CD3e (17A2) BV711, BioLegend, Cat# 100241
CD6 (OX-129) PE, BioLegend, Cat# 146404
CD24 (M1/69) FITC, eBioscience, Cat# 11-0242-82
CD24 (M1/69) BV510, BioLegend, Cat# 101831
CD25 (PC61) PE, BioLegend, Cat# 102008
CD25 (3C7) PE-Dazzle 594, BioLegend, Cat# 102048
CD27 (LG.3A10) PerCp-Cy5.5, BioLegend, Cat# 124214
CD27 (LG-7F9) PE-Cy7, eBioscience, Cat# 25-0271-82
CD44 (IM7) BV605, BioLegend, Cat# 103047
CD44 (IM7) BV711, BioLegend, Cat# 103057
CD45 (30-F11) BV510, BioLegend, Cat# 103138
CD45RB (C363.16A) PerCP-Cy5.5, BioLegend, Cat# 103313
CD69 (H1.2F3) APC, BioLegend, Cat# 104514
CD122 (TM-β1) PE-Cy5, BioLegend, Cat# 123220
IFN-g (XMG1.2) PE-Cy7, eBioscience, Cat# 25-7311-82
IL-17A (TC11-18H10.1) Pacific Blue BioLegend, Cat# 506918
KI-67 (16A8) BV-605, BioLegend, Cat# 652413
TCRd (GL3) APC, eBioscience, Cat# 17-5711-82
TCRd (GL3) BV421, BioLegend, Cat# 118120,
Themis (1TMYS) eFluor 660, eBioscience, Cat# 50-5918-82
Vg1 (2.11) APC, BioLegend, Cat# 141108
Vg4 (UC3-10A6) PE-Cy7, eBioscience, Cat# 25-5828-82
Vg5 (536) FITC, BD Biosciences, Cat# 553229
CD16/CD32 (93), eBioscience, Cat# 14-0161-86
2. in vitro culture:
CD3e (145-2C11), BioLegend, Cat# 100302
CD28 (37.51), eBioscience, Cat# 14-0281-86
3. MACS negative enrichment:
CD19 (6D5), BioLegend, Cat# 115504
CD11b (M1/70), BioLegend, Cat# 101204
CD11c (N418), BioLegend, Cat# 117304
TCRβ (H57-597), BioLegend, Cat# 109204
TER-119 (TER-119), BioLegend, Cat# 116204

Validation

The antibodies used in this study were used according to the manufacturer's recommendation. Validation was based on the description provided on the manufacturer's homepage.
Antibody (Clone), Fluorochrome if applicable, Validation
CD3e (145-2C11) PerCP-Cy5.5, https://www.biolegend.com/fr-fr/products/percp-cyanine5-5-anti-mouse-cd3epsilon-antibody-4191
CD3e (17A2) APC-eFluor 780, https://www.thermofisher.com/antibody/product/CD3-Antibody-clone-17A2-Monoclonal/47-0032-82
CD3e (17A2) BV711, https://www.biolegend.com/fr-fr/products/brilliant-violet-711-anti-mouse-cd3-antibody-10022
CD6 (OX-129) PE, https://www.biolegend.com/en-gb/products/pe-anti-mouse-cd6-antibody-9015
CD24 (M1/69) FITC, https://www.thermofisher.com/antibody/product/CD24-Antibody-clone-M1-69-Monoclonal/11-0242-82
CD24 (M1/69) BV510, https://www.biolegend.com/de-at/products/brilliant-violet-510-anti-mouse-cd24-antibody-9925
CD25 (PC61) PE, https://www.biolegend.com/en-ie/products/pe-anti-mouse-cd25-antibody-424
CD25 (3C7) PE-Dazzle 594, https://www.biolegend.com/fr-fr/products/pe-dazzle-594-anti-mouse-cd25-antibody-10220
CD27 (LG.3A10) PerCp-Cy5.5, https://www.biolegend.com/en-gb/products/percp-cyanine55-anti-mouse-rat-human-cd27-antibody-4396?GroupID=BLG10664
CD27 (LG-7F9) PE-Cy7, https://www.thermofisher.com/antibody/product/CD27-Antibody-clone-LG-7F9-Monoclonal/25-0271-82?ef_id=Cj0KCQiAx9q6BhCDARIsACwUxu6-6R41LHqaHsprCPAQpwhNVjwMYLi9Z92bUenzFejzQijpgDO8N0saAnC7EALw_wcB:G:s&s_kwcid=AL!3652!3!278928759553!!!g!!!1454324556!63404918784&cid=bid_pca_frg_r01_co_cp1359_pjt0000_bid00000_0se_gaw_dy_pur_con&gad_source=1&gbraid=0AAAADxi_GRvB6nH4JC11EpYBSB_CK0fz&gclid=Cj0KCQiAx9q6BhCDARIsACwUxu6-6R41LHqaHsprCPAQpwhNVjwMYLi9Z92bUenzFejzQijpgDO8N0saAnC7EALw_wcB
CD44 (IM7) BV605, https://www.biolegend.com/de-de/products/brilliant-violet-605-anti-mouse-human-cd44-antibody-8807?

GroupID=BLG10425
CD44 (IM7) BV711, https://www.biolegend.com/nl-nl/products/brilliant-violet-711-anti-mouse-human-cd44-antibody-10316
CD45 (30-F11) BV510, https://www.biolegend.com/en-gb/products/brilliant-violet-510-anti-mouse-cd45-antibody-7995
CD45RB (C363.16A) PerCP-Cy5.5, https://www.biolegend.com/de-at/products/percp-cyanine5-5-anti-mouse-cd45rb-antibody-6225?GroupID=BLG259
CD69 (H1.2F3) APC, https://www.biolegend.com/en-ie/products/apc-anti-mouse-cd69-antibody-3169
CD122 (TM-β1) PE-Cy5, https://www.biolegend.com/de-at/products/pe-cyanine5-anti-mouse-cd122-il-2rbeta-antibody-14800
IFN-g (XMG1.2) PE-Cy7, https://www.thermofisher.com/antibody/product/IFN-gamma-Antibody-clone-XMG1-2-Monoclonal/25-7311-82
IL-17A (TC11-18H10.1) Pacific Blue, https://www.biolegend.com/en-ie/products/pacific-blue-anti-mouse-il-17a-antibody-4145?GroupID=GROUP24
KI-67 (16A8) BV-605, https://www.biolegend.com/de-at/products/brilliant-violet-605-anti-mouse-ki-67-antibody-8983
TCRd (GL3) APC, https://www.thermofisher.com/antibody/product/TCR-gamma-delta-Antibody-clone-eBioGL3-GL-3-GL3-Monoclonal/17-5711-82
TCRd (GL3) BV421, https://www.biolegend.com/de-at/products/brilliant-violet-421-anti-mouse-tcr-gamma-delta-antibody-7249?GroupID=BLG3687
Themis (1TMYS) eFluor 660, https://www.thermofisher.com/antibody/product/Themis-Antibody-clone-1TMYS-Monoclonal/50-5918-82
Vg1 (2.11) APC, https://www.biolegend.com/en-gb/products/apc-anti-mouse-tcr-vgamma1-1-cr4-antibody-7218?GroupID=BLG9203
Vg4 (UC3-10A6) PE-Cy7, https://www.thermofisher.com/antibody/product/TCR-V-gamma-2-Antibody-clone-UC3-10A6-Monoclonal/25-5828-82
Vg5 (536) FITC, https://www.bdbiosciences.com/en-us/products/reagents/flow-cytometry-reagents/research-reagents/single-color-antibodies-ruo/fitc-hamster-anti-mouse-v-3-tcr.553229
CD16/CD32 (93) https://www.thermofisher.com/antibody/product/CD16-CD32-Antibody-clone-93-Monoclonal/14-0161-82
CD3e (145-2C11) https://www.biolegend.com/en-gb/products/purified-anti-mouse-cd3epsilon-antibody-28?GroupID=BLG6744
CD28 (37.51) https://www.thermofisher.com/antibody/product/CD28-Antibody-clone-37-51-Monoclonal/14-0281-82
CD19 (6D5) https://www.biolegend.com/en-gb/products/biotin-anti-mouse-cd19-antibody-1527?GroupID=BLG7045
CD11b (M1/70) https://www.biolegend.com/en-gb/products/biotin-anti-mouse-human-cd11b-antibody-346?GroupID=BLG10660
CD11c (N418) https://www.biolegend.com/fr-fr/products/biotin-anti-mouse-cd11c-antibody-1814
TCRβ (H57-597) https://www.biolegend.com/ja-jp/products/biotin-anti-mouse-tcr-beta-chain-antibody-269
TER-119 (TER-119) https://www.biolegend.com/ja-jp/products/biotin-anti-mouse-tcr-beta-chain-antibody-269
The antibodies used in this study were used according to the manufacturer's recommendation. Validation was based on the description provided on the manufacturer's homepage.
Antibody (Clone), Fluorochrome if applicable, Validation
CD3e (145-2C11) PerCP-Cy5.5, https://www.biolegend.com/fr-fr/products/percp-cyanine5-5-anti-mouse-cd3epsilon-antibody-4191
CD3e (17A2) APC-eFluor 780, https://www.thermofisher.com/antibody/product/CD3-Antibody-clone-17A2-Monoclonal/47-0032-82
CD3e (17A2) BV711, https://www.biolegend.com/fr-fr/products/brilliant-violet-711-anti-mouse-cd3-antibody-10022
CD6 (OX-129) PE, https://www.biolegend.com/en-gb/products/pe-anti-mouse-cd6-antibody-9015
CD24 (M1/69) FITC, https://www.thermofisher.com/antibody/product/CD24-Antibody-clone-M1-69-Monoclonal/11-0242-82
CD24 (M1/69) BV510, https://www.biolegend.com/de-at/products/brilliant-violet-510-anti-mouse-cd24-antibody-9925
CD25 (PC61) PE, https://www.biolegend.com/en-ie/products/pe-anti-mouse-cd25-antibody-424
CD25 (3C7) PE-Dazzle 594, https://www.biolegend.com/fr-fr/products/pe-dazzle-594-anti-mouse-cd25-antibody-10220
CD27 (LG.3A10) PerCp-Cy5.5, https://www.biolegend.com/en-gb/products/percp-cyanine55-anti-mouse-rat-human-cd27-antibody-4396?GroupID=BLG10664
CD27 (LG-7F9) PE-Cy7, https://www.thermofisher.com/antibody/product/CD27-Antibody-clone-LG-7F9-Monoclonal/25-0271-82?ef_id=Cj0KCQiAx9q6BhCDARIsACwUxu6-6R41LHqaHsprCPAQpwhNVjwMYLi9Z92bUenzFejzQijpgDO8N0saAnC7EALw_wcB:G:s&s_kwcid=AL!3652!3!278928759553!!!g!!!1454324556!63404918784&cid=bid_pca_frg_r01_co_cp1359_pjt0000_bid00000_0se_gaw_dy_pur_con&gad_source=1&gbraid=0AAAADxi_GRvB6nH4JC11EpYBSB_CK0fz&gclid=Cj0KCQiAx9q6BhCDARIsACwUxu6-6R41LHqaHsprCPAQpwhNVjwMYLi9Z92bUenzFejzQijpgDO8N0saAnC7EALw_wcB
CD44 (IM7) BV605, https://www.biolegend.com/de-de/products/brilliant-violet-605-anti-mouse-human-cd44-antibody-8807?GroupID=BLG10425
CD44 (IM7) BV711, https://www.biolegend.com/nl-nl/products/brilliant-violet-711-anti-mouse-human-cd44-antibody-10316
CD45 (30-F11) BV510, https://www.biolegend.com/en-gb/products/brilliant-violet-510-anti-mouse-cd45-antibody-7995
CD45RB (C363.16A) PerCP-Cy5.5, https://www.biolegend.com/de-at/products/percp-cyanine5-5-anti-mouse-cd45rb-antibody-6225?GroupID=BLG259
CD69 (H1.2F3) APC, https://www.biolegend.com/en-ie/products/apc-anti-mouse-cd69-antibody-3169
CD122 (TM-β1) PE-Cy5, https://www.biolegend.com/de-at/products/pe-cyanine5-anti-mouse-cd122-il-2rbeta-antibody-14800
IFN-g (XMG1.2) PE-Cy7, https://www.thermofisher.com/antibody/product/IFN-gamma-Antibody-clone-XMG1-2-Monoclonal/25-7311-82
IL-17A (TC11-18H10.1) Pacific Blue, https://www.biolegend.com/en-ie/products/pacific-blue-anti-mouse-il-17a-antibody-4145?GroupID=GROUP24
KI-67 (16A8) BV-605, https://www.biolegend.com/de-at/products/brilliant-violet-605-anti-mouse-ki-67-antibody-8983
TCRd (GL3) APC, https://www.thermofisher.com/antibody/product/TCR-gamma-delta-Antibody-clone-eBioGL3-GL-3-GL3-Monoclonal/17-5711-82
TCRd (GL3) BV421, https://www.biolegend.com/de-at/products/brilliant-violet-421-anti-mouse-tcr-gamma-delta-antibody-7249?GroupID=BLG3687
Themis (1TMYS) eFluor 660, https://www.thermofisher.com/antibody/product/Themis-Antibody-clone-1TMYS-Monoclonal/50-5918-82
Vg1 (2.11) APC, https://www.biolegend.com/en-gb/products/apc-anti-mouse-tcr-vgamma1-1-cr4-antibody-7218?GroupID=BLG9203
Vg4 (UC3-10A6) PE-Cy7, https://www.thermofisher.com/antibody/product/TCR-V-gamma-2-Antibody-clone-UC3-10A6-Monoclonal/25-5828-82
Vg5 (536) FITC, https://www.bdbiosciences.com/en-us/products/reagents/flow-cytometry-reagents/research-reagents/single-color-antibodies-ruo/fitc-hamster-anti-mouse-v-3-tcr.553229
CD16/CD32 (93) https://www.thermofisher.com/antibody/product/CD16-CD32-Antibody-clone-93-Monoclonal/14-0161-82
CD3e (145-2C11) https://www.biolegend.com/en-gb/products/purified-anti-mouse-cd3epsilon-antibody-28?GroupID=BLG6744

CD28 (37.51) https://www.thermofisher.com/antibody/product/CD28-Antibody-clone-37-51-Monoclonal/14-0281-82
CD19 (6D5) https://www.biolegend.com/en-gb/products/biotin-anti-mouse-cd19-antibody-1527?GroupID=BLG7045
CD11b (M1/70) https://www.biolegend.com/en-gb/products/biotin-anti-mouse-human-cd11b-antibody-346?GroupID=BLG10660
CD11c (N418) https://www.biolegend.com/fr-fr/products/biotin-anti-mouse-cd11c-antibody-1814
TCRβ (H57-597) https://www.biolegend.com/ja-jp/products/biotin-anti-mouse-tcr-beta-chain-antibody-269
TER-119 (TER-119) https://www.biolegend.com/ja-jp/products/biotin-anti-mouse-tcr-beta-chain-antibody-269

Animals and other research organisms

Policy information about studies involving animals; ARRIVE guidelines recommended for reporting animal research, and Sex and Gender in Research

Laboratory animals	C57BL/6J mice were purchased from the Charles Rivers Laboratories. Double Ifng-YFP.Il17a-GFP reporter mice were generated and bred in house by crossing the following single reporter strains: Great (Ifng-YFP) (https://doi.org/10.1038/ni.1715) obtained from the Jackson Laboratory, and IL17-GFP (https://doi.org/10.1038/ni.2416), from Biocytogen, LLC. CD6ΔD3/ΔD3 and Themis-/- mouse strains were established at A.M. Carmo (https://www.biorxiv.org/content/10.1101/2022.04.29.490054v1) and R. Lesourne's (https://doi.org/10.1038/ni.1768) laboratories, respectively. All mice used were adult (6-14 weeks). Mice were bred and housed in rooms with a light-dark cycle of 14h/10h, temperature of 22-24 °C and relative humidity of 45-65% in SOPF (specific opportunistic pathogen free) animal holding rooms and used for experimental purposes in SPF (specific pathogen free) animal rooms of the Instituto de Medicina Molecular João Lobo Antunes Rodent Facility (Lisbon, Portugal).
Wild animals	No wild animals were used in this study.
Reporting on sex	Findings do not apply to one sex: both male and female mice were used in this study. Sex-matched mice were used for each individual experiment. Data in Extended Data Figure 4 is based on samples from male mice, given the analysis of cells from testis.
Field-collected samples	No field-collected samples were used in this study.
Ethics oversight	All experiments involving animals were approved by the Animal Welfare Body of Instituto de Medicina Molecular João Lobo Antunes (ORBEA-iMM), set up in accordance with Portuguese law (article 34 of Decreto-Lei 113/2013, transposed from the European Directive 2010/63/EU), and submitted to the local competent authority Direcção-Geral de Alimentação e Veterinária (DGAV) for authorization.

Note that full information on the approval of the study protocol must also be provided in the manuscript.

Plants

Seed stocks	n/a
Novel plant genotypes	n/a
Authentication	n/a

Flow Cytometry

Plots

Confirm that:

☒ The axis labels state the marker and fluorochrome used (e.g. CD4-FITC).

☒ The axis scales are clearly visible. Include numbers along axes only for bottom left plot of group (a 'group' is an analysis of identical markers).

☒ All plots are contour plots with outliers or pseudocolor plots.

☒ A numerical value for number of cells or percentage (with statistics) is provided.

Methodology

Sample preparation	The cell preparation protocols, with detailed biological source of the cells, are provided in the Materials and Methods section.
Instrument	Cell sorting was performed using one of the following Cell Sorters (all from BD Biosciences): BD FACSAria IIu (red, blue and violet lasers), III (red, yellow-green, blue and violet lasers) or Fusion (red, yellow-green, blue and violet lasers). Flow cytometry analysis was performed on a FACS Fortessa X-20 (red, yellow-green, blue and violet lasers), LSRFortessa (red,

yellow-green, blue and violet lasers) or Cytek Aurora (red, yellow-green, blue and violet lasers, or additionally ultraviolet laser).

Software

All flow cytometry data were acquired using FACSDiva 6.2 or FACSDiva 8.0 (BD Biosciences), except for Themis protein expression data, which were acquired using SpectroFlo (Cytek). Cell sorting was performed using FACSDiva 6.1.3 or FACSDiva 9.0 software (BD Biosciences). All flow cytometry data were analysed using FlowJo v10.7.2 software (FlowJo LLC)

Cell population abundance

Post-sort sample purity was examined by flow cytometry. Samples containing at least 95% of desired population were used for further analysis.

Gating strategy

Using FSC/SSC, debris were removed. Doublet exclusion was performed at least once by using FSC-A versus FSC-W. Additionally, for cell-sorting, double exclusion was further performed by using SSC-A versus SSC-W. Non-viable cells were then excluded by the inclusion of a viability dye in the staining. Gating strategies to identify cell populations of interest include:
gamma-delta T cells: CD3ε+TCR+
gamma-deltaIFN YFP+ cells: CD3ε+TCR+YFP+
gamma-delta17 GFP+ cells: CD3ε+TCR+GFP+
gamma-deltaDN cells: CD3ε+TCR+YFP-GFP-
gamma-delta17 GFP+Vg4+ cells: CD3ε+TCR+Vg4+GFP+
gamma-delta17 GFP+Vg1-V4- cells: CD3ε+TCR+Vg1-Vg4-GFP+
gamma-deltaIFN YFP+Vg1+ cells: CD3ε+TCR+Vg1+GFP+
gamma-deltaIFN YFP+Vg4+ cells: CD3ε+TCR+Vg4+GFP+
CD27+ gamma-delta T cells: CD3ε+TCR+CD27+
CD27- gamma-delta T cells: CD3ε+TCR+CD27-
CD44-CD45RB- gamma-delta T cells: CD3ε+TCR+CD24-CD44-CD45RB-
CD44highCD45RB- gamma-delta T cells: CD3ε+TCR+CD24-CD44highCD45RB-
CD45RB+CD44+ gamma-delta T cells: CD3ε+TCR+CD24-CD45RB+CD44+
IFN-g+ gamma-delta T cells: CD3ε+TCR+IFN-g+

☒ Tick this box to confirm that a figure exemplifying the gating strategy is provided in the Supplementary Information.